


Characterization of the intracellular acidity regulation of brain tumor cells and consequences for therapeutic optimization of temozolomide

Alaa Tafech, Pierre Jacquet, Céline Beaujean, Arnold Fertin, Yves Usson, Angélique Stéphanou* 

Univ. Grenoble Alpes, CNRS, UMR 5525, VetAgro Sup, Grenoble INP, TIMC, 38000 Grenoble, France

* Correspondence: angelique.stephanou@univ-grenoble-alpes.fr

Simple Summary: Tumor cells have a high metabolic activity which makes the environment around them more acidic. This acidic environment encourages the aggressiveness, and invasiveness of the tumor, which is linked to a worse prognosis. Cancer cells may control in different ways their internal acidity when exposed to the acidic environment. In this study two types of brain tumor cells were exposed to different levels of acidity to characterize their response in terms on intracellular pH regulation. The results show that these cells don't handle acidity the same way. One cell type can reduce its internal acidity, while the other can withstand higher acidity levels. The ability to manage acidity seems to depend on the specific cell type and involves various mechanisms to keep the cells working properly. This study explored these cells in both 2D flat layers and 3D structures called spheroids. In spheroids, the regulation process of internal acidity appears to work differently than in 2D. These findings could influence treatment because the temozolomide drug used to fight brain tumors works better in certain pH environments. By adjusting the pH outside the cells, the effectiveness of the drug can be improved. This suggests that personalized treatment might be possible by combining temozolomide with substances that control pH.

Abstract: A well-known feature of tumor cells is high glycolytic activity leading to acidification of the tumor microenvironment through extensive lactate production. This acidosis promotes processes such as metastasis, aggressiveness and invasiveness that has been associated to a worse clinical prognosis. Moreover, the function and expression of transporters involved in regulation of intracellular pH might be altered. In this study the capacity of tumor cells to regulate their intracellular pH when exposed to a range of pH from very acidic to basic, has been characterized in two glioma cell lines, F98 and U87, using a new recently published method of fluorescence imaging. Our result show that the tumor regulation of acidity is not the same for the two cell lines, U87 cells are able to reduce their intracellular acidity whereas F98 cells do not exhibit this property. On the other hand F98 cells show a higher resistance to acidity than U87 cells. Intracellular acidity regulation appears highly cell-dependent where different mechanisms are activated to preserve the cell integrity and functioning. This characterization was performed on 2D monolayer cultures and 3D spheroids. Spatial heterogeneities were exhibited in 3D suggesting a spatially modulated regulation in this context. Based on the corpus of knowledge available in the literature, we proposed plausible mechanisms to interpret our results together with some new lines of investigation to validate our hypotheses. Our results might have implications on therapy since the activity of temozolomide is highly pH-dependent. We show that the drug efficiency can thus be enhanced depending on the cell type by manipulating the extracellular pH. Personalized treatment could be considered by the combination of temozolomide with pH-regulating agents.

Citation: Tafech A.; Jacquet P.; Beaujean C.; Fertin A.; Usson Y.; Stéphanou A. Characterization of the intracellular acidity regulation of brain tumor cells. *Preprints* 2023, 1, 0. <https://doi.org/>

Copyright: © 2023 by the authors. Submitted to *Preprints* for possible open access publication under the terms and conditions of the Creative Commons Attribution (CC BY) license (<https://creativecommons.org/licenses/by/4.0/>).

Keywords: BCECF probe, fluorescence microscopy, glioblastoma, pH regulation, resistance to acidity, temozolomide

1. Introduction

Acidity is a well-known feature of the tumor microenvironment. It is observed in a variety of solid tumors [1–3]. The pH can be very heterogeneous within the same tumor, with localized acid zones. pH measurements using electrodes have shown that the pH

can reach 5.9 in brain tumors, with an average value at around 6.8 while the pH in normal brain tissue is around 7.1 [1].

Tumor cells that proliferate abnormally quickly run out of oxygen and become hypoxic. In hypoxia, the cells are not able to produce ATP via OXPHOS. In order to adapt to this harmful environment, HIF signaling shifts energy production towards anaerobic glycolysis, allowing hypoxic tumor cells to continue to produce ATP despite the low oxygen levels. Due to their significant fermentation activity, hypoxic tumor cells secrete a large amount of lactate and H^+ ions, which can lead to changes in the intracellular pH (pH_i) of cancer cells. To help deal with the excess production of lactate and H^+ ions, tumor cells activate a number of pH regulating proteins to export lactate and H^+ ions and keep the pH_i within the physiological level. Once excreted, lactate and H^+ ions induce a decrease in extracellular pH (pH_e) leading to acidification of the tumor microenvironment [3–6].

Tumor cells are generally associated with alkaline pH_i values of 7.1 to 7.6 and acidic pH_e values of 6.2 to 6.9 [7], whereas, normal cells are found with a lower pH_i (7.0–7.2) than that in the environment in physiological conditions (7.3–7.4) [8,9]. As a consequence there is an inverse pH gradient for tumor cells. The fact that pH_i is significantly higher than pH_e in tumors demonstrates the existence of powerful mechanisms to prevent acidification of the intracellular environment [10–12]. The tools used by tumor cells to regulate their pH_i are varied and depend on the cell type. Several pH regulatory proteins show increased expression (often modulated by the transcription factor HIF-1) or activity in tumor cells. These redundant proteins of tumor pH regulation include: Na^+/H^+ exchangers (NHEs) such as NHE1 [13], Vacuolar-type Adenosine TriPhosphatase (V-ATPase) [14], the monocarboxylate transporters (MCTs) such as MCT1, MCT2, MCT3, and MCT4 [15], Carbonic Anhydrases such as CAII, CAIX, and CAXII [13,16], and the HCO_3^- transporters [17]. Distinct mechanisms can also be set up in cells with different invasive or metastatic potentials [18,19]. A different subcellular localization of pH regulators has been demonstrated in a model of brain tumors [20].

It has become evident that pH_i is an important regulator of metabolism and many cell functions such as cell proliferation [21–23], cell cycle progression [24,25] and differentiation [26,27]. The inverted pH gradient is considered a hallmark of cancer [28], which promotes tumor growth, invasion, and metastasis of cancer cells via various mechanisms. Therefore it appears that the measurement of pH_i in tumors can be of interest for monitoring the progression of cancers and the responses of cancer cells to various treatments.

Despite advances in the development of new therapeutic strategies, a major underlying factor in cancer-related death remains treatment resistance. The cytoplasmic membrane functions as a semi-permeable physical barrier that separates the intracellular and extracellular environment. Small and uncharged molecules can easily diffuse through the membrane, while the passage of charged molecules is more difficult since the membrane is polarized. On the other hand, the diffusion of chemotherapeutic agents can be altered by changes in the pH of the tumor environment. For instance, the acidic pH_e increases the cellular uptake of weakly acidic drugs such as chlorambucil [29] and melphalan [30] and thus increases the efficacy of the drugs. In contrast, the acidic pH_e retards the uptake of weakly basic drug such as doxorubicin [31,32] and mitoxantrone [33,34], the extracellular acidity that can be found in the tumor microenvironment can limit their passage through the membrane of cancer cells, compromising their anti-tumor efficacy. Extracellular acidity may also play a role in drug resistance by increasing the activity of P-glycoprotein (P-gp), which is involved in drug efflux. Activation of the p38 MAP Kinase signaling pathway by acidity is involved in the activation of P-glycoprotein. Therefore, inhibition of the p38 pathway restores the sensitivity of tumor cells to chemotherapeutic agents.

Cancer drug research and development initially focused on targeting cancer cell proliferation. It then appeared that the environment could also be taken into account. The role of acidity in the evolution and therapeutic response of tumors has been particularly documented and much attention is currently paid to strategies targeting this tumor acidity. The different strategies that directly target tumor acidity or exploit characteristics of acidity are now being developed and have begun to show promising results.

A first strategy targeting tumor acidity consists in studying drugs that can be activated under acidic conditions to have a better specificity of the treatment. We cite for example the molecule temozolomide (TMZ), used against glioblastoma [35]. Another strategy is to inhibit the various proteins involved in maintaining pH_i , which is crucial for the survival of tumors in an acidic environment, using small molecule inhibitors or antibodies. Targeted proteins include NHEs, MCTs, CAs, NBCs (Na^+/HCO^- co-transporters) and V-ATPase [36–38]. Tumor acidity is also exploited in the development of nanoparticles which release cytotoxic agents under acidic condition, encountered in the tumor tissue [39,40].

In this study we characterized the regulation of intracellular acidity of brain tumor cells for two cell lines, F98 murine glioma and U87 human glioblastoma. This was performed using fluorescence microscopy with the pH-dependent fluorescent probe BCECF, for which we recently developed a new methodology that extends the pH range measurements and accuracy [41]. Measurements were performed on 2D cell cultures and on 3D spheroids. Differences were highlighted between the two cell lines and some hypotheses were proposed to explain them. Finally, the impact of the extracellular pH on TMZ efficacy was investigated on the two cell lines with the aim to identify the optimum pH range for each.

2. Materials and Methods

2.1. Cell lines

U-87 MG and F98 cell lines from ATCC were used. The U87 cell line was established from a human glioblastoma. The cells are often polynuclear with very fine membrane extensions. Their mean doubling time is 30.8 ± 2.5 [42]. The F98 cell line is a murine glioma. The cells are predominantly spindle shaped and have an *in vitro* doubling time of approximately 18 hours [43]. Both cell lines are cultured in the same conditions in plastic flasks. The culture medium is composed of DMEM with 4.5% glucose, supplemented with 10% fetal bovine serum and 2 mM glutamine (Dutscher, Bernolsheim, France). The cells are maintained at 37°C in a humid atmosphere with 5% CO_2 . For the experiments, cells were seeded at a concentration of 1000 cells/well in 96-well flat CleaLine® plates for 2D monolayer cultures or in 96-well CELLSTAR® round bottom ultra-low attachment plates for 3D spheroid cultures.

2.2. Microscope

A laser scanning confocal microscope Zeiss LSM 710 was used. It is an inverted microscope especially suited for live cell imaging experiments, equipped with an incubation chamber to maintain physiological conditions with a 37°C temperature and 5% CO_2 . It is equipped with the following 6 laser lines : Diode 405 nm, Argon 458 nm, 488 nm, 514 nm and Helium-Neon 543 nm, 633 nm.

2.3. pH measurements

The fluorescent pH-sensitive probe BCECF (2',7'-bis(carboxymethyl)-5(6)-carboxyfluorescein) purchased from ThermoFischer Scientific was used for pH measurements. The fluorescent excitation profile is pH-dependent. The shape of the emission spectra remains almost constant with a main emission peak. A ratiometric pH measurement is implemented so that pH determination is independent of the probe concentration or optical path length because pH is related to the ratio (in excitation or emission) at two characteristic wavelengths. In our

case, two excitation wavelengths were used and the fluorescence emission is measured at one wavelength for each excitation. The ratio (R) of the fluorescent intensities measured for these two emission wavelengths is monitored as a function of the pH to construct the curve $R = f(pH)$ (see Appendix A). For our measurements we exploited the best combination of emission wavelengths obtained with the dual excitation at 405 nm and 488 nm based on a methodology we recently developed to optimize the quality of the measurements [41]. We have found that the best method to measure the intracellular pH of F98 cells is to set the emission wavelength at 517 nm for the 405 nm laser and 546 nm for the 488 nm laser. In this case the pH is monitored as a function of the fluorescence ratio $R = I_{517nm} / I_{546nm}$. Whereas for U87 cells, the intracellular pH is measured by fixing the emission wavelength at 556 nm for the 405 nm laser and at 517 nm for the 488 nm laser. In this case the pH is monitored as a function of to the fluorescence ratio $R = I_{517nm} / I_{556nm}$.

We note that for intracellular pH measurements, BCECF-AM was used. The added acetoxymethyl ester (AM) group makes the probe neutral, allowing it to cross cell membranes. Once inside the cell, intracellular esterases will cleave the ester group of the molecule, releasing the charged groups and trapping the probe in the cytoplasmic compartment [44,45]. The BCECF devoid of the AM group cannot enter the cells and remains in the extracellular compartment.

2.4. Loading cells with pH probes

The fluorescent probe was loaded into cells thanks to its cell-permeable ester derivative that is hydrolysed by cytosolic esterases to yield fluorescent intracellularly trapped probe. Suspended cells were cultured in 96 well flat bottom ultra low attachment plates (Dominique Dutscher, France). They are seeded on day 1 at a density of 1×10^3 cells per well in a volume of 200 μ L of complete medium and allowed to adhere for 48 hours before experiment. After that, cells were incubated in serum-free DMEM medium with 5 μ M of probe prepared from a 1 mM stock-solution in DMSO, for 30 minutes at 37°C and 5% CO₂. FBS serum may contain endogenous esterase activity. Therefore, loading medium should be serum-free to keep extracellular hydrolysis of the AM ester to a minimum. Once loaded with the probe, cells were washed three times at 37°C, to remove the probe not taken up by the cells, with 200 μ L of serum-free DMEM of the pH that was desired for the observation.

2.5. Intracellular pH calibration

The calibration of the intracellular pH is based, after loading the cells with the pH probe, on an equilibrium of the intracellular pH (pH_i) with the extracellular pH (pH_e) of the culture medium which value is known. In other words, it consists in imposing the pH_i at known values and determining for each of these values the fluorescence ratio (as described above). To impose the pH_i , the addition of nigericin in the culture medium, whose ionic composition in K^+ is similar to that of the treated cells, allows to equilibrate the intracellular pH with the pH of the medium by creating a membrane antiport K^+ / H^+ . Therefore, as a first step, the calibration solutions are prepared so that they contain a concentration of 90 mM of K^+ ions and 5 μ M of nigericin. The pH is adjusted by adding 0.1 M HCl or 0.1 M NaOH in order to obtain solutions in a pH range of 4 to 9. For each cell line, the ratio of fluorescence intensities is monitored as a function of pH and the curve $R = f(pH_i)$ is constructed (see Appendix A).

2.6. pH measurements in spheroids

Spheroids were cultured in CELLSTAR® 96 well, round bottom ultra-low attachment plates. F98 and U87 cells were seeded on day 1 at a density of 1×10^3 cells per well in a volume of 200 μ L of medium. The cells are always maintained at standard culture conditions in an incubator at 37°C in a humid atmosphere, composed of 95% air and 5% CO₂. 24 hours after plating, spheroids are formed (1 spheroid per well).

pH_i measurements were initiated on day 4 by adding 5 μM of BCECF-AM to the culture medium. After 60 min of incubation with BCECF-AM, spheroid were washed 3 times with fresh medium (pH ~ 7.4) to remove the probes not taken by the cells. The spheroids were then exposed to different DMEM media with three different pH_e values (5.00, 6.00 and 7.40).

Eight hours after incubation with a given pH_e, confocal fluorescence images were recorded by successively exciting each spheroid at 405 nm and 488 nm. Starting from one pole of each spheroid, the excitations are carried out by optical sections along the Z axis (confocal z-stack) through the spheroid with a Z-slice spacing of 5 μm between adjacent optical planes. With our confocal setup, light penetration into the spheroid was limited to 150 μm depth.

To monitor the pH_i in spheroids, the fluorescence images were processed as follows: the background signal, taken from an empty region, was subtracted from the measurements, and the ratio of emission intensity resulting from excitation at the two wavelengths (405 nm and 488 nm) was calculated pixel-to-pixel. To convert the ratio signals to pH_i values in the spheroids, the appropriate calibration curves obtained for 2D cell cultures were used.

We note that pH_e values could not be measured in the interstitial liquid between the cells inside the spheroids since we could not detect any extracellular BCECF signal in the spheroid mass. This may be related to the limited diffusion of the BCECF molecules through the spheroid mass into the interstitial liquid due to the high cell density.

In total, 18 spheroids were treated including the two cell lines F98 and U87. All measurements were made based on three replicates for each pH_e values considered (5.00, 6.00 and 7.40) and for each cell line. The most representative replicate in each case is presented for illustration.

2.7. Assessment of cell resistance to acidity

In order to assess *in vitro* the cells resistance to pH_e changes, cells were seeded at a concentration of 5 × 10⁴ cells/mL into a 24-well plate and incubated for 48 hours at 37°C in a humid atmosphere containing 5% CO₂. After 48 hours of growth, the culture medium was removed and replaced with the test medium with a pH_e ranging from 4 to 9. To assess cell mortality, the trypan blue stain was used. Trypan blue stains dead and dying cells whose membrane integrity is damaged. The culture medium was removed from each well and 200 μL of trypsin was added per well to remove the cells. The removed cells were then re-suspended in 800 μL of culture medium. The cell suspensions were diluted 1:1 (v:v) with 0.4% trypan blue and then a 10 μL mixture was transferred to a cell count slide. Cell mortality was monitored using an automated cell counter over a period of 72 hours and the number of dead cells was measured every four hours for each pH_e tested.

2.8. Measure of cell viability after TMZ treatment

Viability after temozolomide (TMZ) treatment under different pH_e was evaluated using MTT test. The cells were seeded on day 1 in a 96-well plate at the rate of 1 × 10⁴ cells per well in 200 μL of culture medium. On day 3, the cells were incubated 48 hours with TMZ in different extracellular pH for a final volume of 100 μL per well. At the end of the incubation period, 10 μL of an MTT solution was added to achieve a final concentration of 0.5 mg/mL. The cells were then incubated for 3 hours at 37°C, 5% CO₂ and protected from light. The Formazan crystals formed after incubation were dissolved by adding 100 μL of dimethylsulfoxide to each well. Finally, the amount of live cells was quantified by an absorbance reading at 570 nm. The viability is expressed as a percentage of living cells relative to the control.

In spheroid cultures, the cell viability was evaluated by confocal microscopy using two probes: the BCECF probe, used as a powerful probe that allows labelling all the cells, and the Sulforhodamine B probe (SRB, purchased from ThermoFischer Scientific), that marks in red the dead cells. The difference between these two fluorescent signals provides the relative amount of living cells in the spheroid. The spheroids are grown for 3 days and are then exposed to TMZ for 48 hours. The spheroids are then incubated for one hour with $5\mu\text{M}$ of BCECF and $10\mu\text{M}$ of SRB before image acquisition.

2.9. Evaluation of IC_{50} of TMZ

The TMZ IC_{50} value, *i.e.* the TMZ concentration that results in 50% cell viability, was evaluated for the two cell lines using the MTT test. The cells were incubated in standard culture medium at physiological $\text{pH}=7.4$ for 48 hours with the following TMZ concentrations: 0, 50, 100, 200, 300, 400, 500, 1000 μM . Viability was measured as the mean of 3 replicates for each tested concentrations. The IC_{50} values measured were 200 μM and 250 μM for F98 and U87 cells respectively.

2.10. TMZ treatment

The cell lines in 2D cell culture and in spheroids are exposed to TMZ during 48 hours. TMZ is solubilized using DMSO. The experiments are thus carried in the three following experimental conditions: with TMZ, with DMSO only, without TMZ and DMSO. The control is taken as the DMSO so as to evaluate the effect of TMZ only.

2.11. Statistical analysis

All experiments were performed with three replicates. All the data points are presented as the mean and standard deviation (SD) of these three replicates. The number of replicates is not big enough to perform a reliable statistical analysis. As a consequence, the results presented should be considered as an overall trend, not a definitive confirmation. We made one exception with the evaluation of the temozolomide since we performed *paire-wise* experiments amenable to a statistical paired t-test that we employed to compare the mean of 3 paired biological repeats. Significant differences are defined as $P < 0.05$.

3. Results

3.1. Intracellular pH changes in cell cultures

The two cell lines F98 and U87 were first exposed to instantaneous extracellular pH changes. At time $t = 0$ the extracellular pH (pH_e) of the culture medium with pH at 7.4 was changed by a culture medium with a new pH_e . Eighteen different pH_e values were considered from 5 to 8.4 with 0.2 increments. For each new pH_e , the changes in the intracellular pH (pH_i) were monitored every hour over a period of 8 hours. Confocal fluorescence images were recorded by exciting the cells internalized BCECF probe at 405 nm and 488 nm successively. The intensity ratio of the two emission wavelengths was calculated pixel-to-pixel and the pH_i was thus determined using the calibration curves (Appendix A).

Parallel measurements were conducted to measure the evolution of the pH_e using the non-permeable version of the BCECF. It is indeed known that the pH of the culture medium is not stable over time, unless a buffer is used [41]. Since we aimed to characterize spontaneous pH_i adaptation, we chose not to regulate the pH_e with a buffer to avoid constraining the overall system.

Beforehand, the basal pH_i of each cell line, in their physiological culture medium at $\text{pH}_e=7.4$, was measured. In this basal initial condition, pH_i is 7.65 ± 0.13 for F98 cells and 7.48 ± 0.12 for U87 cells.

Figure 1(A,B) shows the effect of pH_e change on the pH_i of F98 and U87 cells as a function of time. On the short term (~ 1 hour), the sudden change of pH_e creates a shock

on the cells since the pH_i of both cell lines almost instantly takes the value of the pH_e . After that, the pH_i regulation process takes 2 hours to produce some effect and one more hour to reach a stationary state. On the longer term, after 4 hours and up to 8 hours, the pH_i remains stable and is specific to the cell line.

Figure 1(C,D) shows the simultaneous measurements of the pH_e which exhibit a similar drift for both cell culture media. At this time scale of 8 hours the variations of the pH_e is independent of the presence of the cells [41].

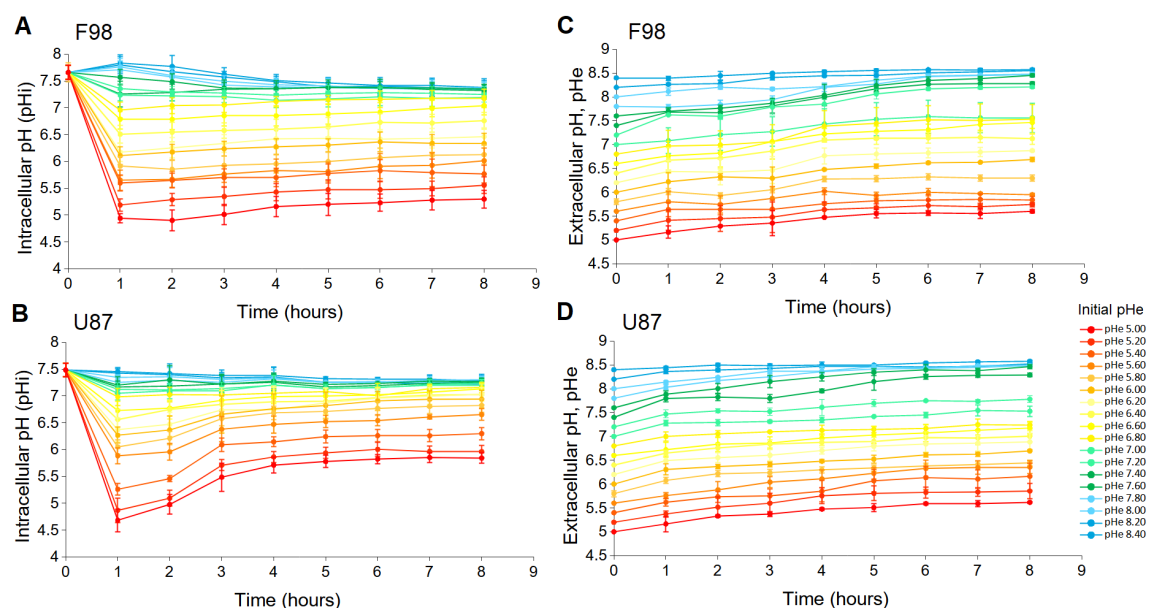


Figure 1. Evolution of the pH_i for sudden changes of the extracellular pH from 5 to 8.4 for F98 cells (A) and U87 cells (B). Simultaneous evolution of the pH_e of the culture medium of F98 cells (C) and U87 cells (D). Each measure points are mean (\pm SD) of three independent experiments.

By combining figures 1.A and 1.C and figures 1.B and 1.D, a pH_e value can be associated to a corresponding pH_i value measured at the same instant. This relationship between pH_e and pH_i is displayed in Figure 2 for the two cell lines. It allows to integrate the pH_e drift.

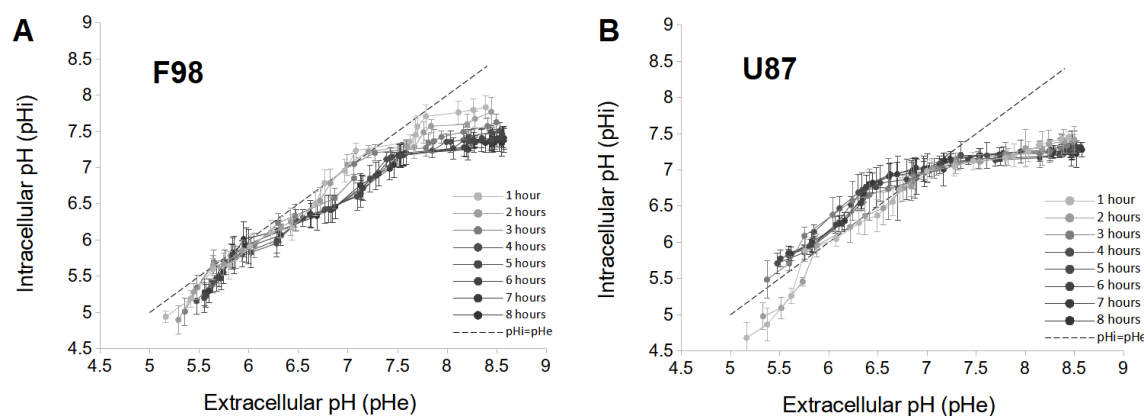


Figure 2. Relationship between pH_e and pH_i of F98 (A) and U87 (B) cells plotted at each hour from 1 to 8 hours. Each measure points are mean (\pm SD) of three independent experiments.

pH changes in F98 cells

For F98 cells, the pH_i is almost always lower than the pH_e , especially as time increases (Fig.2.A). For this cell line, there is no inversion of the pH gradient as usually documented in tumor cells [46]. In addition, a quasi-linear increase in pH_i with pH_e in the range [5.0-7.2] is observed, and the values of the pH_i are very close to those of the pH_e . Moreover, the dependence of pH_i as a function of time is low in the acidic pH_e range, as the curves are almost superimposed. However, the range with the higher pH_e values, shows a marked dependence of the pH_i with time: in the first 4 hours, the pH_i of F98 cells decreases sharply and stabilizes after 5 hours. At that time, the relationship between pH_i and pH_e exhibits a plateau for pH_e above 7.2. F98 cells have therefore the ability to progressively adjust with time their pH_i under basic conditions (above 7.2).

pH changes in U87 cells

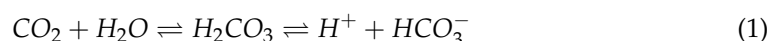
For U87 cells, in the range of pH_e [5.0-6.8], the pH_i is higher than the pH_e which is in agreement with the reverse pH gradient described in tumor cells (Fig.2, B) [46]. U87 cells are therefore able to increase their pH_i under acidic condition. In addition, a time dependence of pH_i is also noted in this pH_e range: the pH_i increases over 3 hours before being less influenced after 4 hours. However, in the zone of $pH_e > 6.8$, the pH_i is always smaller than the pH_e and the pH_i is completely independent of time (superimposed curves). U87 cells have therefore the ability to rapidly maintain a pH level close to the physiological one for pH_e above 6.8.

Interpretation

At their basal state, *i.e.* at the physiological pH of the culture medium, F98 cells have a pH_i of 7.65 ± 0.13 . Lowering the pH_e to 5.00 rapidly decreases the pH_i to 4.94 ± 0.08 (after 1 hour). This decrease of the pH_i corresponds to the rise of hydrogen ions (H^+) inside the F98 cells.

The main mechanism responsible for pH_i changes is the movement of H^+ ions across the plasma membrane([47–49]). Extracellular acidification stimulates the passive influx of H^+ ions into the cell by increasing the permeability of the plasma membrane, resulting in a decrease in pH_i [50]. As acidic pH_e limits the availability of bicarbonate ions (HCO_3^-) and thereby reduces both passive and dynamic HCO_3^- -dependent buffering, tumor cells are thought to use the sodium-hydrogen exchanger (NHE exchanger) to recover from intracellular acidification. However, their poor recovery during this assay suggests that NHE activity is low in F98 glioma cells. This is in agreement with the study by Glunde *et al.*, 2002 [51], which showed that extracellular acidification inhibits the activity of NHE-1 exchanger (sodium-hydrogen exchanger isoform-1) in glioma cell lines (C6 and F98).

For basic pH_e , F98 cells maintain a physiological level of pH_i around 7.4, more precisely 7.33 ± 0.13 . Going from an initial state of pH_i 7.65 ± 0.13 to 7.33 ± 0.13 , a passive influx of H^+ ions into the cell is imposed. Although basic pH_e limits the availability of H^+ ions in the culture medium, H^+ ions are generated by the hydration of CO_2 according to the reaction:



Inside the cells, the H^+ ions entering the cells will be sequestered by the bicarbonate ions (HCO_3^-), thus increasing the pH_i . This is, however, not the case with F98 cells. As the F98 cells have lowered their pH_i , it can be assumed that the F98 cells used the Cl^- / HCO_3^- exchanger to export the HCO_3^- ions outside the cells. Once the HCO_3^- ions are exported, H^+ ions are no longer sequestered leading therefore to a decrease in pH_i . The Cl^- / HCO_3^-

exchanger has been identified as an essential regulator particularly activated following an alkaline incubation [52–54]. Activation of $\text{Cl}^-/\text{HCO}_3^-$ exchanger decreases the rate of acidification during recovery of pH_i from extracellular alkaline incubation.

At their basal state, U87 cells have a pH_i of 7.48 ± 0.12 . Lowering the pH_e , to 5.00, decreases pH_i to 4.75 ± 0.14 (after 1 hour). First, the rapid drop in pH_i is due to the passive influx of H^+ ions into the cell. However, unlike F98 cells, U87 cells have reduced their intracellular acidity to 5.81 ± 0.12 after 8 hours. Therefore, considering the low HCO_3^- -dependent buffering at acidic pH , it can be suggested that U87 cells used the dynamic NHE exchanger to recover from intracellular acidification. The plasma membrane isoforms of this protein extrude one intracellular H^+ ion in exchange for one extracellular Na^+ ion, leading thus to an increase in pH_i .

For basic pH_e , U87 cells maintain a pH_i level close to physiological pH , more precisely 7.25 ± 0.03 . Going from an initial state of pH_i 7.48 ± 0.12 to 7.25 ± 0.03 , U87 cells use, like the F98 cells, the $\text{Cl}^-/\text{HCO}_3^-$ exchanger to export the HCO_3^- ions outside the cells and to recover from alkaline incubation by decreasing pH_i . The temporal dependence of pH_i observed with F98 cells can be explained by the fact that the pH_i of F98 cells at time zero is higher than that of U87 cells (by about 0.2 pH units).

3.2. Resistance to extracellular pH changes

Many recent studies have shown that the cancer cells exhibit a higher resistance to acidity due to a better ability to regulate their pH_i [55–57]. As we end up with two tumor cell lines that do not regulate their acidity in the same way, we were interested in evaluating the effects of acidification of the tumor microenvironment on the mortality of those glioma cells.

Cell resistance to instantaneous external pH changes was assessed by measuring cell mortality every 4 hours for 72 hours, *i.e.* until mortality level is higher than 90% for all tested experimental conditions. The measurements were performed according to the protocol described in section Materials and Methods. Two graphical representations for the results are used. The first shows the evolution of the percentage of dead cells (over the entire number of cells of the population) with time (Fig.3.(A,B)). The second represents the excess mortality compared to the control (which is the standard culture medium with a physiological pH of 7.4) (Fig.3.(C,D)). These curves are obtained by subtracting the control to each curve of figures 3.(A,B) where the control is now set to 100%. We note that if the excess mortality is lower than 100% then the mortality is reduced compared to the control condition.

Results are shown in Figure 3. Both cell lines resist to high acidic conditions over 48 hours and, at least 15% of cells are alive. After 72 hours, the cells are almost all dead (Fig.3.(A,B)). At 28 hours, F98 mortality is higher for initial extreme acidic (4.00) and basic (9.00) pH_e with a mortality of approximately 53% and 60% respectively. However, U87 mortality is higher for acidic pH_e with cell mortality of approximately 60%, 54% and 51% at initial pH_e 4.00, 5.00 and 6.00, respectively. Beyond 28 hours, cell mortality becomes more important and the excess mortality, compared to the control state, reaches nearly 125% for certain pH_e (Fig.3.(C,D)). F98 cells appear to have a higher resistance to acidity than U87 cells, whereas, U87 cells have a higher resistance to basicity than F98 cells.

Several studies have reported the existence of a link between the regulation of intracellular acidity and the reduction of cell death [58–61]. Therefore, in order to minimize the toxic intracellular acidity, tumor cells must regulate the H^+ ions extrusion mechanisms which increase the pH_i . Taking these considerations into account, U87 cells that regulate intracellular acidity should exhibit lower cell mortality than F98 cells that do not regulate intracellular acidity. However, that is not the case here. U87 cells exhibit higher mortalities

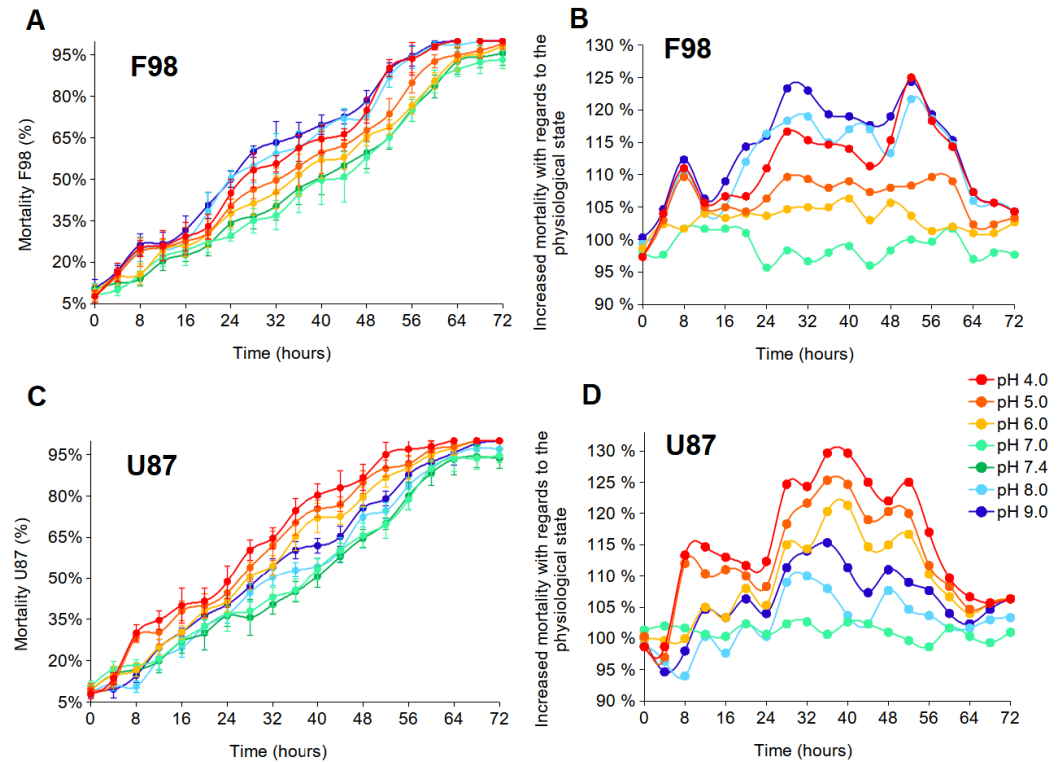


Figure 3. Effects of pH_e on cell mortality of F98 and U87 cells. (A,B) show the evolution of the percentage of dead cells (over the entire number of cells of the population) with time. Each measure points are mean (\pm SD) of three independent experiments. (C,D) show the excess mortality compared to the control set at 100% (which is the standard culture medium with an initial physiological pH of 7.4).

under acidic conditions. In this case, the regulation of intracellular acidity does not seem to constitute an adaptive response since the regulation of acidity does not protect from death. The pH regulation process might be too costly to the cell.

3.3. Intracellular pH in spheroids

In this section, experiments on spheroid were considered. Their 3D structure leads to spatial heterogeneities [62] associated to the limited diffusion of oxygen and nutrients from the periphery to the core [63,64]. The cells of a spheroid thus experience a radial gradient of oxygen often associated to a reverse radial gradient of acidity since hypoxic cells are the source of acidity. Moreover, contrary to the 2D culture conditions, cells in a spheroid are in close contact and cell-cell binding interactions influence the ability of the cells to adapt to the extracellular environment and to resist death. pH_i spatial heterogeneity is therefore assessed in this 3D context for the two cell lines.

Under identical culture conditions, F98 spheroids (diameter 430-490 μm) are larger than U87 spheroids (diameter 290-330 μm) (Fig.4). It has been reported that the size of spheroids, ranging from tens to hundreds of microns in diameter, is critical for cellular functions and model applications, thus spheroids of different sizes do not exhibit the same properties [65]. For example, spheroids with a diameter $< 150 \mu\text{m}$ will not develop chemical gradients (pH_i , oxygen concentration, etc.). These gradients are usually generated in spheroids with diameters $> 200 \mu\text{m}$ and increase with increasing spheroid size [65,66]. Therefore, due to a size-induced oxygen difference, larger pH_i gradient are expected in F98 spheroids than in U87 spheroids. Moreover, F98 spheroids are much more spherical than U87 spheroids with a denser and more compact shape. Therefore, the nature of cell-cell

interactions is probably different between the two cell lines.

439
440

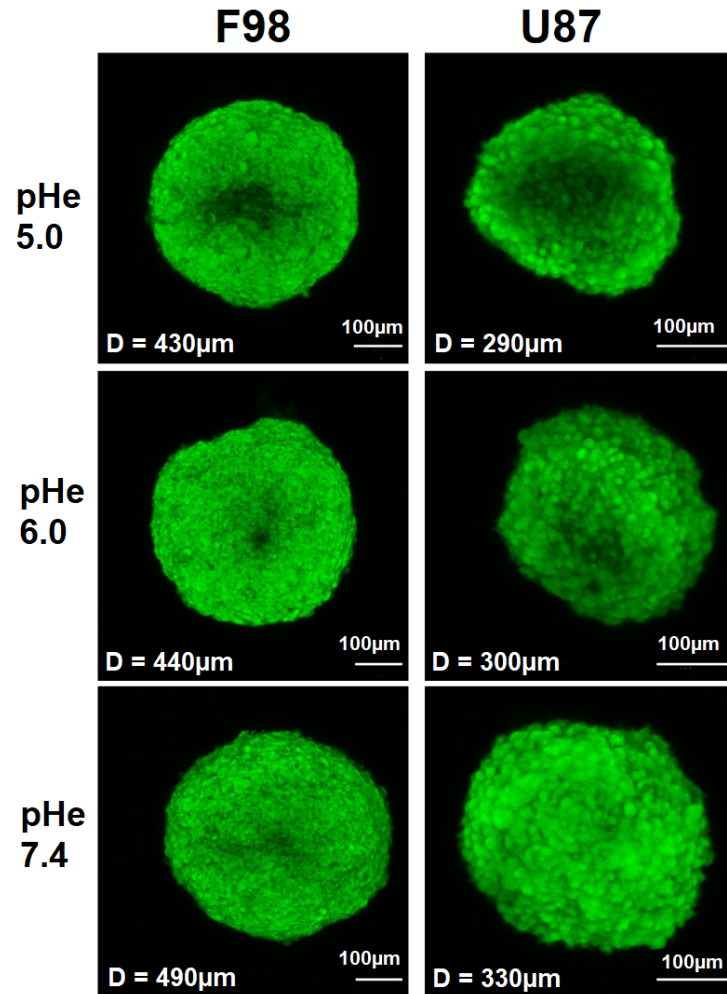


Figure 4. Fluorescent images of the spheroids generated by first collecting a stack of fluorescent images with a step size of $5 \mu\text{m}$ along the Z-direction and projected them down to a high quality 2D-image by summing the slices. The spheroids were incubated at different initial pH_e values and confocal Z-stak images were recorded 8 hours after incubation. Scale bar = $100 \mu\text{m}$

Figure 5 shows the pH_i map in the slice located at a depth of $85 \mu\text{m}$ in F98 and U87 spheroids. The pH maps exhibit a pH_i gradient with its lower value at the center of the slice. F98 spheroids, larger than U87 spheroids, exhibit a more irregular pH_i gradient than U87 spheroids which is "smoother". These gradients are directly correlated to the depletion of oxygen, from the periphery to the core of the spheroid, since the pH_i measured at the center are systematically lower than the pH_e (taken at 8 hours). We recall that the DMEM culture medium undergoes a pH drift which values are summarize in table 1.

441
442
443
444
445
446
447
448

For a quantitative analysis, the pH_i maps (Fig.5) were processed in two ways: first the distribution of the pH_i measured for each pixel as a function of the pixel distance from the center of the spheroid was plotted (Fig.6). The added value of this representation is to retain the spatial information contained in the pH_i map. Second, the pH_i maps of the spheroids have been segmented to delineate 3 zones: a central zone, an intermediate zone and a peripheral zone (Fig.7). A mean pH_i value is associated with each zone. The following two paragraphs are dedicated to these two types of analysis.

449
450
451
452
453
454
455
456

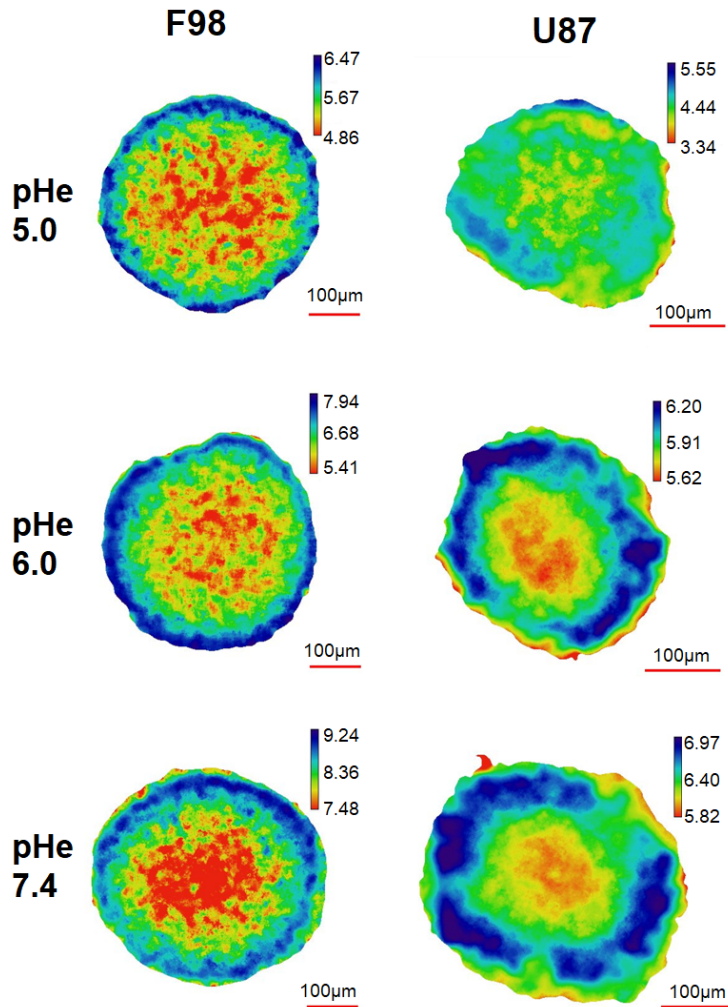


Figure 5. pH_i map in the slice located at a depth of 85 μm for F98 (on the left) and U87 (on the right) spheroids. The spheroids were exposed to three different pH_e conditions for 8 hours. Scale bar = 100 μm.

pH distribution

The distribution of the pH_i measured for each pixel as a function of the pixel distance from the center of the spheroid is represented in figure 6 for the two cell lines exposed to three different initial pH_e (5.00, 6.00 and 7.40). Each point on the pH_i distribution represents a pixel of the map with pixel size 1.24 μm for F98 and 0.83 μm for U87. Pixel sizes are much smaller than the size of a cell, as a consequence, cellular heterogeneity can be assessed since a cell has pH_i values that spread over several pixels. In addition, on the pH_i distribution, the color code indicates the density of superimposed pixels.

The pH_i distributions of F98 spheroids (Fig.6, left graphs) show a wide dispersion of points in the spheroids. However, this dispersion becomes less important approaching the center and the periphery. The majority of cells located at a distance ranging from 100 μm to 200 μm from the center have a pH_i between [5.00-5.50], [5.50-6.50] and [8.00-9.00] when incubated at initial pH_e of 5.00, 6.00 and 7.40, respectively. However, by following the evolution of the pH_i as we move away from the center of the spheroid, we can see that a large group of cells tend to increase their pH_i above 5.50 and 6.50 for initial pH_e of 5.00 and 6.00, respectively. On the other hand, and under basic conditions, although the majority of F98 cells located near the center of the spheroid have a pH_i between [8.00-9.00], a small

Initial pH_e	pH_e (t=8h)	pH_e (t=48h)
5.00	5.60	6.07
6.00	6.60	6.91
6.40	7.12	7.33
6.80	7.53	7.67
7.20	7.88	8.15
7.40	8.20	8.52

Table 1. pH drift of DMEM medium after 8 hours and after 48 hours at 37°C and 5% CO₂

group of cells tend to decrease their pH_i below 8.00. It appears that the F98 cells located around 150 μ m from the center of the spheroid, attempt to regulate their pH_i towards the physiological state.

The pH_i distributions of U87 spheroids (Fig.6, right graphs) show a dispersion of points much less important than F98 cells and which follows lines of higher density with increasing pH as we move away from the center of the spheroid. Hence the distribution of pH_i is much more homogeneous in the U87 spheroids. In addition, depending on the point density, the majority of points have a pH_i between [4.00-4.50], [5.00-6.00] and [6.00-6.00] when incubated at initial pH_e of 5.00, 6.00 and 7.40, respectively. Therefore, U87 cells do not regulate their pH_i and are more acidic than F98 cells in a spheroid.

It has been reported that pH_i depends on the adhesive interactions of cells with neighboring cells and cell-cell contact interactions regulate cell activities *via* modulation of pH_i [67,68]. The fact that central F98 cells tend to regulate their pH_i may be associated with an increase in the number of cell-cell contacts inside the spheroid.

Since tumor spheroids represent heterogeneous 3D structures in terms of pH_i , in which the cells of the outer proliferative layer have a more alkaline pH_i than the quiescent cells inside [69], pH_i measurements were performed separately for the inner and outer layers of the spheroids. For this, the pH_i maps of figure 5 were used to produce a spheroid outline. This contour was used to generate 3 concentric, non-overlapping layered regions of interest (ROI) of width equal to a third of the spheroid radius (Fig.7). ROI_c, ROI_m and ROI_p are defined as the center, intermediate and peripheral ROI respectively. A mean pH_i value is therefore associated with each zone. Radial pH_i data are summarized in Figure 8.

pH_i in ROI

Analysis of pH_i separately in the core and on the periphery of the F98 spheroids showed a significant difference between the central and peripheral parts (Fig.8.A). Quantitative analysis of the pH_i values revealed that the pH_i in the central areas was 5.08 ± 0.21 , 5.87 ± 0.28 and 7.51 ± 0.31 for spheroids incubated at initial pH_e of 5.00, 6.00, 7.40, respectively. Whereas, the pH_i in peripheral parts of these spheroids was 5.97 ± 0.21 , 7.18 ± 0.33 and 8.57 ± 0.27 , respectively. F98 spheroids showed therefore 0.89, 1.31 and 1.06 units of difference in pH_i between the center and the periphery, when incubated at initial pH_e of 5.00, 6.00 and 7.40 respectively. Regardless of pH_e , F98 spheroids develop therefore significant radial gradients of pH_i , with the lowest levels reached at the core.

In U87 spheroids, quantitative analysis of the pH_i values revealed that the mean pH_i in the central areas was 4.17 ± 0.16 , 5.72 ± 0.04 and 6.06 ± 0.08 for spheroids incubated at initial pH_e of 5.00, 6.00, 7.40, respectively (Fig.8.B). Whereas, the pH_i in peripheral parts of these spheroids was 4.41 ± 0.25 , 6.03 ± 0.09 and 6.65 ± 0.20 , respectively. U87 spheroids showed therefore 0.24, 0.31 and 0.59 units of difference in pH_i between the center and the periphery, when incubated at initial pH_e 5.00, 6.00 and 7.40 respectively. According to an-

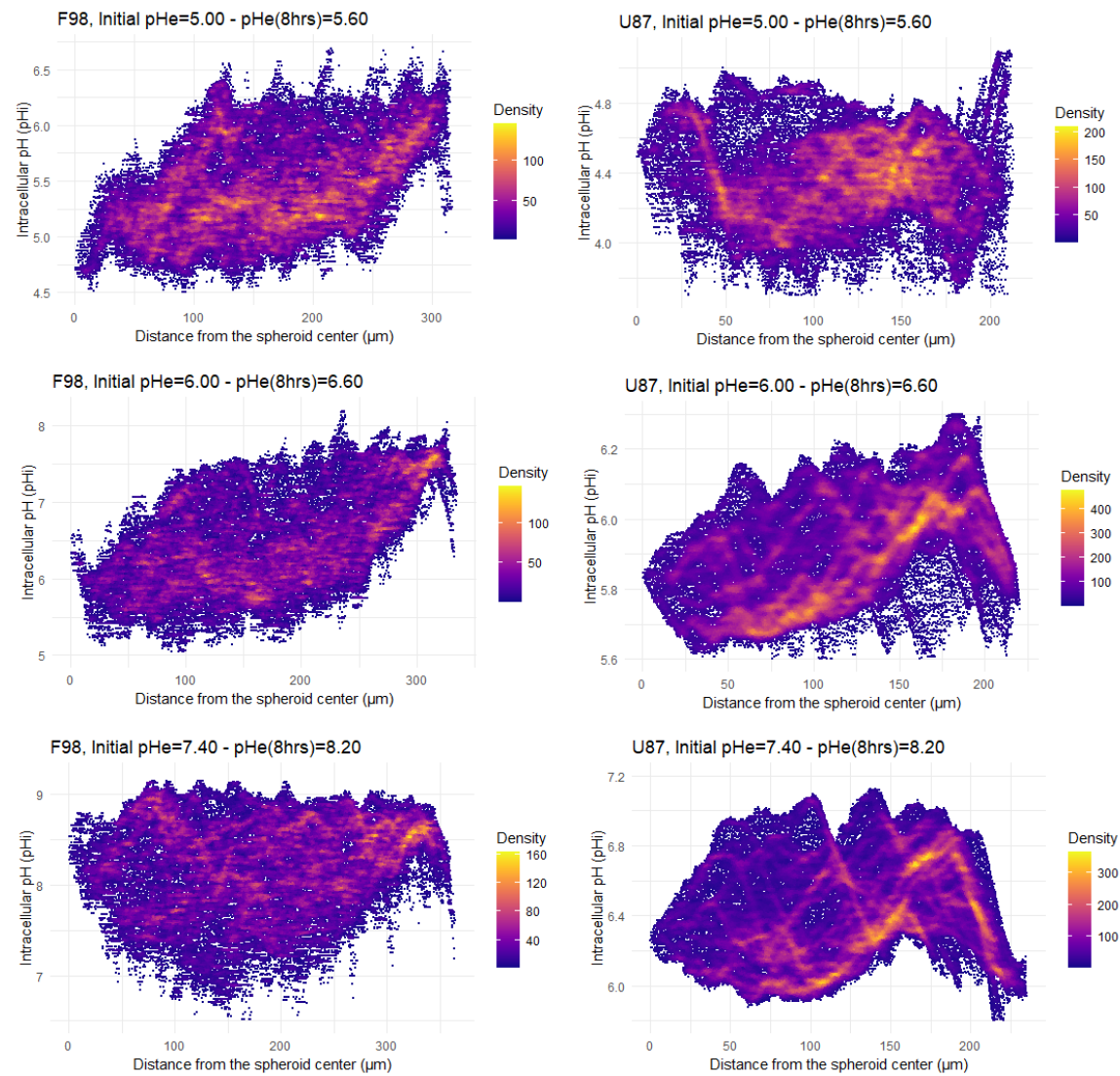


Figure 6. Radial profiles of pH_i distribution after 8 hours of incubation of F98 (left) and U87 (right) spheroids. Each point corresponds to a pixel in the pH_i map and, each pixel has a pH_i value and is located at a certain distance from the center of the spheroid. All the pixels from the pH_i maps are displayed.

other observation, the gradient of pH_i decreases with decreasing pH_e and the distribution becomes quasi-homogeneous under very acidic conditions. 520

To compare the pH_i gradients between the two spheroids F98 and U87, the slope of each gradient was calculated (Fig.8). F98 spheroids show a pH_i gradient with a slope of 0.53, 0.66 and 0.44 when incubated at a pH_e of 5.60, 6.60 and 8.20 respectively. While the U87 spheroids show a pH_i gradient with a slope of 0.29, 0.15 and 0.12 when incubated at a pH_e of 5.60, 6.60 and 8.20 respectively. For a given pH_e , U87 spheroids present pH_i gradients with always a smaller slope than those obtained for the gradients of F98 spheroids. This verifies what we expected, based on the bigger size and density of F98 spheroids. 521 522 523 524 525 526 527 528 529 530

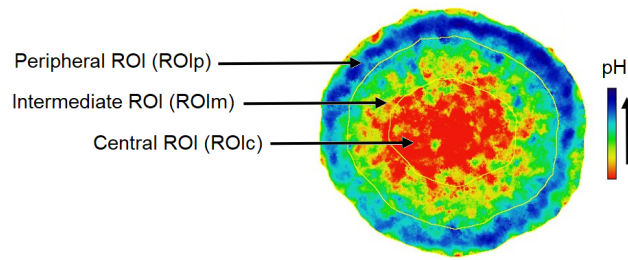


Figure 7. The contour of the spheroid was used to generate three regions of interest (ROI) of width equal to a third of the spheroid radius. ROI_c , ROI_m and ROI_p are defined as the center, intermediate and peripheral ROI respectively.

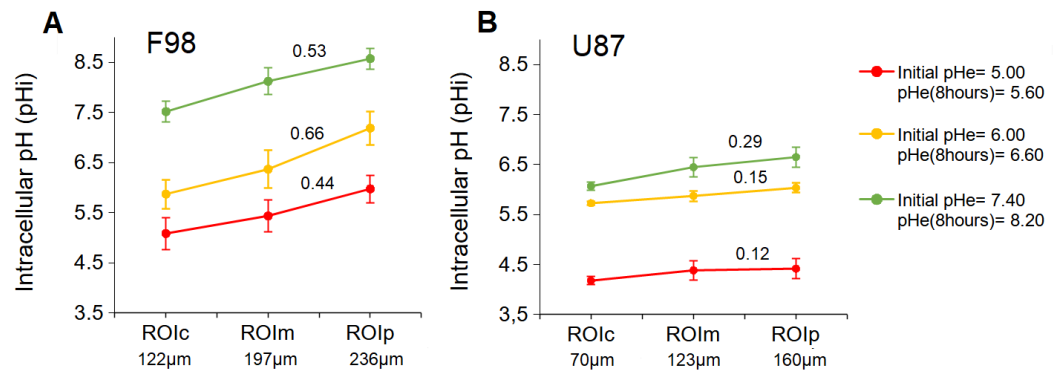


Figure 8. Mean pH_i gradient in F98 (A) and U87 (B) spheroids for three initial pH_e as a function of the ROI from center to periphery.

2D vs 3D cultures

In order to compare the results obtained in 2D cultures and 3D spheroids, the relationship between pH_e and pH_i obtained in these two types of culture (8 hours after incubation at a given pH_e) was plotted on the same graph (Fig.9).

Under acidic and neutral conditions, the peripheral F98 cells show a response quite similar to that of the cells in 2D cultures. Under basic conditions, peripheral cells tend to raise their pH_i compared to the 2D model. Having already assumed that the F98 cells in the 2D cultures used, under basic conditions, the Cl^- / HCO_3^- exchanger to export the HCO_3^- ions outside the cells, we can therefore hypothesize that the activity of the Cl^- / HCO_3^- exchanger is inhibited in 3D cultures.

However, whatever the pH_e , the U87 cells show a completely different activity compared to the 2D cultures. In the spheroid, U87 cells tend to lower their pH_i compared to the 2D model. We have already assumed that the U87 cells in the 2D cultures used, under acidic conditions, the Na^+ / H^+ exchanger to export the H^+ ions outside the cells. The fact that the U87 cells lowered, under acidic conditions, their intracellular pH can be explained by the inhibition of this exchanger, the H^+ ions are therefore conserved in the cells. However, unlike F98 cells, the decrease in pH_i under basic conditions allows us to hypothesize that U87 cells "overexpress" Na^+ / H^+ in the spheroid configuration.

3.4. Effect of pH on temozolomide efficacy

Temozolomide (TMZ) is currently the standard treatment for glioblastoma (GBM) since it is one of the rare molecules able to cross the blood brain barrier. However, there are serious drawbacks, mainly related to the invasive nature of this tumor, and to the inherent and acquired resistance, which can ultimately lead to treatment failure. Therefore, there is an urgent need for novel therapeutic strategies that enhance the benefits of TMZ in terms of

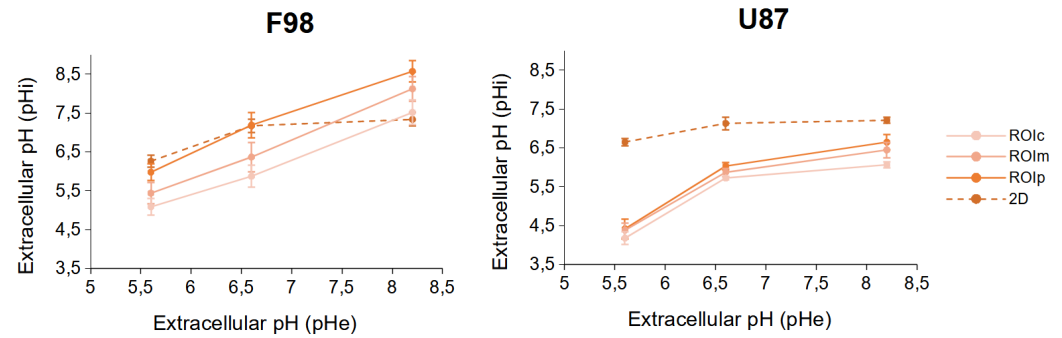


Figure 9. Relationship between pH_e and pH_i of F98 (A) and U87 (B) cells incubated in 2D cultures (dotted lines) and in the three ROI of the spheroids (straight lines). The cells are incubated at different initial pH_e values and the pH_i was measured 8 hours after incubation. Each data point is the mean and SD of three replicates.

patient survival and quality of life.

The effect of TMZ is highly pH dependent [70]. TMZ is stable under acidic conditions. It is converted into its active form in a two step process at physiological and basic pH conditions. However, since tumor cells can acidify their microenvironment, this may influence the efficacy of TMZ. Therefore, there is only a small pH range favoring TMZ-induced damage in tumor cells [35]. In this context, the influence of the extracellular pH (pH_e) on the efficiency of the TMZ complex is studied here in order to determine the optimal pH_e for its use on the two cell lines of interest, F98 and U87.

The majority of previously published drug toxicity research was conducted using commercially available cell media with a pH above 7, which is typical of healthy tissues. These experiments do not reflect the actual conditions of pathological cell division and growth. Therefore, to perform biological experiments under conditions similar to cancer cells, it is important to adjust the pH of cell media to the appropriate value. The experiments in this work were carried out in neutral and acidified cell media and the influence of pH on the toxicity results on the U87 and F98 cell lines was evaluated.

Figure 10 shows the dependence of TMZ toxicity on the pH_e of the medium itself, 48 hours after exposure for the two cell lines in 2D cell cultures and in spheroids. We recall that the pH_e is subjected to a drift over the 48 hours which values are summarized in table 1. The results first show that in most of the cases, there is no significant difference between cultures with DMSO alone and cultures without DMSO.

Table 2 summarizes the results presented in figure 10. The cell viability is evaluated in each case by comparison with the control case taken as the initial physiological $pH_e=7.4$ with DMSO. For values above 100% there is an enhanced viability compared to the control case. This happens for untreated F98 cells in 2D cultures at initial $pH_e=7.2$ and in untreated spheroids for both cell lines at initial $pH_e=6$.

In order to estimate the optimum pH_e for TMZ efficacy, the cell viability gap that measure the difference between the control and TMZ treated cells viabilities is calculated. The higher the gap, the most effective the therapy. The results are presented in figure 11.

For both cell lines in 2D cell cultures (Fig.11(A,B)), the toxicity of TMZ decreases with the decrease of the pH_e value and a pH_e of 8.52 provides a good efficiency of the drug. Interestingly, F98 cells exhibit higher sensitivity toward TMZ treatment at initial pH_e of 6.80 compared to U87. The cell viability is 47 points for F98 cells while it is 21 points for U87

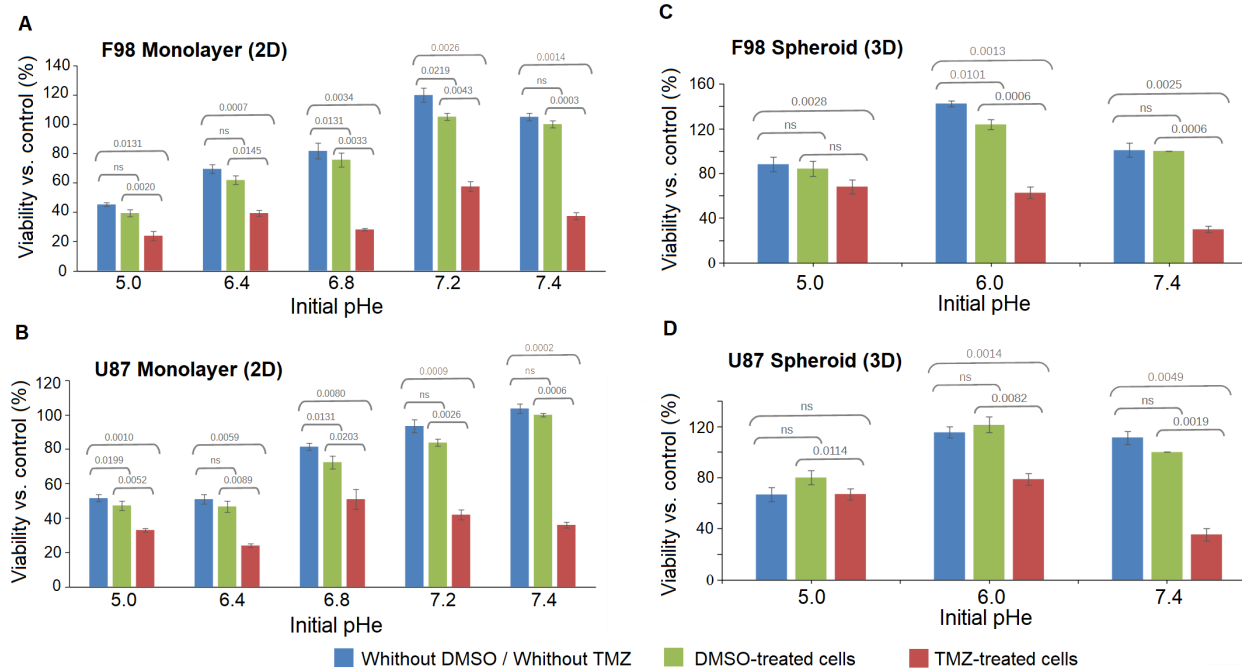


Figure 10. The dependence of TMZ toxicity on the initial pH_e of the medium itself for the two cell lines F98 (top) and U87 (bottom) on 2D monolayer cultures (A,B) and on 3D spheroids (C,D). The control value is taken at pH_e=7.4 with DMSO. Measure points are mean (\pm SD) of three replicates. The statistical paired t-test was employed to compare the means of the viability of three biological repeats for each experimental conditions at each initial pH_e. Significant differences are defined as $P < 0.05$.

cells. For the other pH_e values whether lower or higher, both cell lines behaved similarly. U87 and F98 cells show low sensitivity to TMZ at initial pH_e 6.00 and 6.40 with viability gaps below 25 points. For both cell lines, the optimal pH_e for TMZ efficiency is obtain for the initial pH_e of 7.40 with a drift to 8.52 over the 48 hours of treatment. Since the pH drift usually occur in a few hours, and assuming that a cell viability gap above 40 points is significant enough, the optimal pH_e range for TMZ efficiency is [7.67-8.52] for F98 cells, while it is [8.15-8.52] for U87 cells.

596
597
598
599
600
601
602
603

	Extracellular pH (pH _e)	% cell viability with DMSO (Control)	% cell viability after TMZ treatment	cell viability gap
F98 Monolayer (2D)	6.91	39.28 ± 2.38	23.80 ± 3.31	15
	7.33	61.90 ± 3.14	39.28 ± 2.09	22
	7.67	75.79 ± 4.81	28.17 ± 0.68	47
	8.15	105.15 ± 2.47	57.53 ± 3.43	48
	8.52	100 ± 2.99	37 ± 2.47	62
U87 Monolayer (2D)	6.91	47.30 ± 2.74	32.93 ± 2.74	14
	7.33	48.30 ± 3.11	23.95 ± 3.11	23
	7.67	72.45 ± 3.73	50.89 ± 3.73	21
	8.15	83.83 ± 2.07	41.91 ± 2.07	41
	8.52	100 ± 1.03	35.92 ± 1.03	64
F98 Spheroid (3D)	6.07	84.44 ± 7.21	68.27 ± 3.58	16
	6.91	123.13 ± 7.89	62.27 ± 4.72	60
	8.52	100 ± 8.64	29.83 ± 6.81	70
U87 Spheroid (3D)	6.07	80.49 ± 6.89	67.99 ± 5.36	12
	6.91	121.73 ± 6.21	78.11 ± 5.29	43
	8.52	100 ± 3.31	35.62 ± 4.84	64

Table 2. Quantitative values corresponding to the results displayed in figure 10 and calculation of the cell viability gap presented in figure 11.

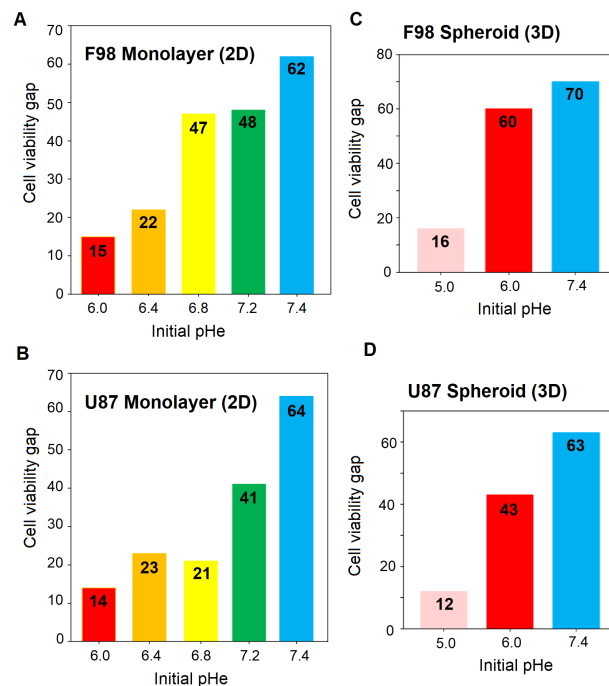


Figure 11. Cell viability gap after TMZ treatment of F98 and U87 for 2D monolayer cultures (A,B) and 3D spheroids (C,D). The cell viability gap is evaluated as the difference between the % cell viability before treatment (DMSO control) and the % cell viability after TMZ treatment

Toxicity on spheroids

Figure 12 presents fluorescent images of F98 and U87 spheroids exposed to a change of pH_e after 3 days of growth. Spheroids were then exposed to DMSO only or to TMZ for 48 hours. The images show that TMZ treated spheroids are smaller at all initial pH_e for the F98 cells (Fig.12.A). On the other hand, U87 cells appears less sensitive to TMZ, and the size reduction appears more important as the initial pH_e increases (Fig.12.B).

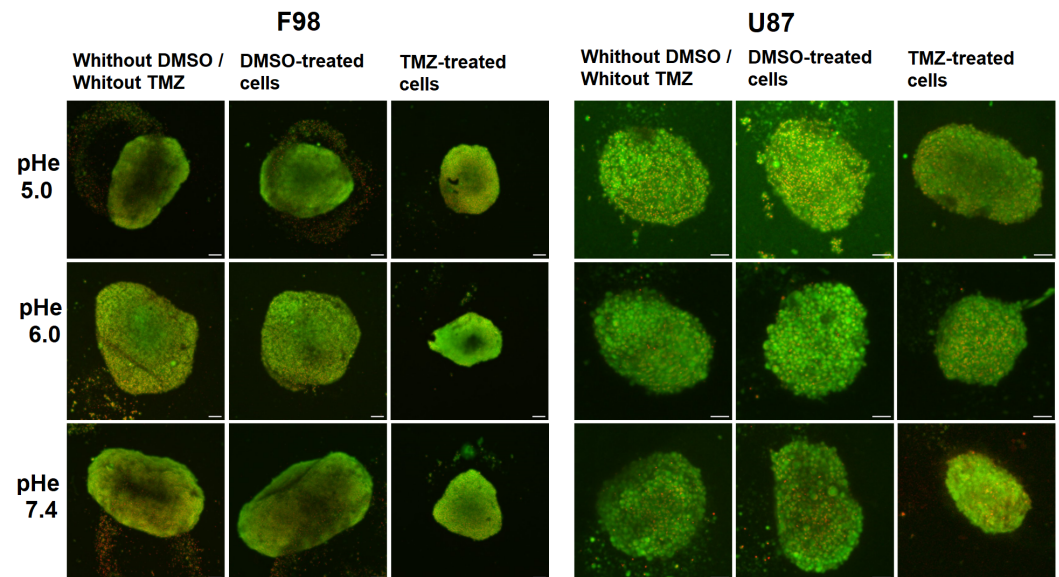


Figure 12. Fluorescent images showing the effect of TMZ on F98 spheroids (A) and on U87 spheroids (B) under different initial pH_e conditions, without DMSO/without TMZ, with DMSO only, with TMZ. Cells are marked in green with BCECF (pH_i indicator) and dead cells are marked in red with SRB. Scale bar= 100 μm

The cell viability gap, *i.e.* the difference between the control and TMZ treated cells viabilities show for both cell line a pH-dependent increase towards higher pH. As expected from the fluorescence images, the TMZ toxicity is more marked for F98 cells than U87 cells with viability gaps of 60 and 70 points for F98 spheroids (Fig.11.C), against 43 and 63 points for U87 spheroids (Fig.11.D) at initial pH_e 6.00 and 7.40 respectively. For the lowest initial pH_e of 5.00, the efficiency of TMZ is reduced for both cell lines, since TMZ is not activated under acidic conditions.

If we compare TMZ efficacy in 2D cultures and 3D spheroids, a discrepancy exists at initial pH_e 6.00. For both cell lines, the TMZ efficacy is very small in 2D cultures and significant in spheroids. In 2D cultures, the cells are homogeneously exposed to a pH_e evolving from 6.00 to 6.91 due to the pH drift. This acidic pH tends to maintain the TMZ in its inactive form. On the other hand in spheroids, there is relatively good efficacy of the TMZ with a cell viability above 40 with a higher mortality for F98 cells. Considering the pH_i gradients in figure 5, we observe that the intracellular pH values can reach values close to basicity (as the pH_e drift is higher at 48 hours). The TMZ effect is more important on F98 cells, which is coherent with the fact that the spheroids are bigger and more compact which gives rise to a more spreaded pH_i gradient, with a population of cells presenting a TMZ sensitive pH. On the other hand, U87 spheroids are smaller and much more homogeneous in terms of cells pH_i , a smaller population is TMZ sensitive.

Overall the results show that the efficacy of TMZ is modulated depending on the cell type, which gives an argument to consider pH_e as a personalized therapeutic target.

4. Discussion

Tumor metabolism has gained renewed attention recently as the acidity generated by tumor cells has been found to be responsible for increase cell aggressiveness favoring invasion and resistance to treatment [71]. The true nature of cancer cell metabolism has become an active source of debate whether it should be considered as an evolutionary specialization, an atavistic remanence [72] or a contextual adaptation to extreme conditions [73–75].

In order to survive the dynamic nature of pH in tumors, cancer cells require the ability to sense tiny pH changes and respond appropriately to maintain pH_i homeostasis. In other words, it is the ability to regulate pH_i . Regulation of pH_i starts with changes in the expression or activity of several plasma membrane molecules such as pumps and transporters that facilitate protons efflux. Thus, a strength in understanding the pH_i regulation of tumors is the understanding of proton transport across the plasma membrane. Therefore, we have experimentally characterized in monolayer cultures the pH_i -regulating capacity of two glioma cell lines using fluorescence microscopy. We observed that the pH_i regulation is not the same for the two cell lines. Firstly, under acidic conditions, U87 human glioblastoma cells are able to reduce intracellular acidity by exporting protons outside the cells. In other words, U87 cells are able to regulate acidic pH. We assumed that U87 cells used the NHE-1 exchanger to export protons in exchange with Na^+ ions. However, we found that F98 cells are not able to regulate acidic pH and H^+ ions have been maintained inside cells. Therefore, another mechanism might be involved since high pH_i degrades intracellular proteins and prevents normal functioning of the cell machinery. On the other side, we found that both cell lines are able to regulate basic pH. We hypothesized that the cells used the Cl^-/HCO_3^- exchanger to export the HCO_3^- ions outside the cells and thus maintain a pH_i level close to the physiological one.

F98 cells that do not regulate intracellular acidity preserve protons inside the cells. In turn, the intracellular protons will produce a toxic effect on many cellular processes such as enzyme activities, metabolism, and gene expression, thus leading to cell death [76,77]. However, this is not the case with F98 cells. F98 cells showed a high resistance to intracellular acidity. Accumulating evidence suggests that in addition to the well characterized ion pumps and exchangers in the plasma membrane, cancer cell lysosomes allow to avoid potentially toxic acidification of the intracellular milieu [78–80]. The lysosome is an intracytoplasmic organelle responsible for the degradation and recycling of intra- or extracellular components. It is very heterogeneous in its size and essentially contains 50 to 60 hydrolases (phosphatases, glycosidases, lipases, nucleases, sulfatases and proteases) active at acidic pH. It has been reported that the pH of lysosomes is maintained at 4.5–5 and the concentration of H^+ ions in lysosomes is almost 1000 times higher than in the cytosol [80,81]. Therefore, the lysosome is not only a place of protein degradation but also a storage compartment for H^+ ions. The pH of lysosomes is regulated by V-ATPase, a pump located in the membrane of these organelles, which brings H^+ ions into these vesicles and acidifies the contents. We suggest that H^+ ions are encapsulated in F98 cells, we therefore assume that F98 cells activate at acidic pH the V-ATPase pump to bring H^+ ions into the lysosomes.

In figure 13, we present a graphical summary of the hypotheses we make - based on the corpus of knowledge available in the literature - about the mechanisms possibly involved in the regulation of intracellular acidity for the two cell lines. This aims to provide an interpretation of the results we obtained, but these hypotheses remain to be verified.

U87 cells that are found to regulate intracellular acidity use the NHE exchanger to export H^+ ions outside the cells. Fluxes through the NHE are driven only by the combined chemical gradients of Na^+ and H^+ and therefore do not directly consume metabolic energy [82]. However, it has been found that the presence of physiological levels of ATP in certain

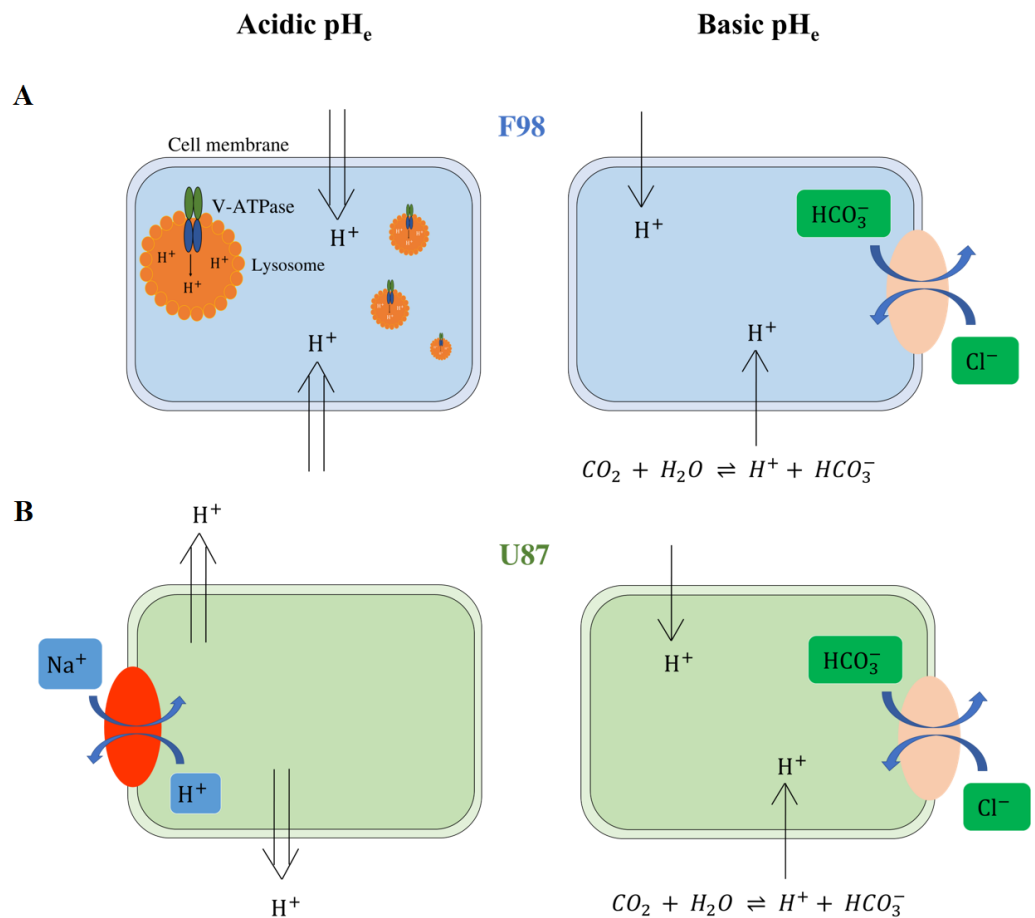


Figure 13. Hypotheses for the mechanisms of intracellular pH_i regulation of F98 (A) and U87 cells (B). F98 cells are not able to regulate acidic pH and H⁺ ions remains inside the cells. To resist acidity, we make the hypothesis that the F98 cells activate the V-ATPase pump to encapsulate the protons in lysosomes. On the other hand, U87 cells are able to regulate intracellular acidity by exporting protons outside the cells. We assume that U87 cells use the NHE-1 exchanger to export protons in exchange with Na⁺ ions. Both cell lines are able to regulate basic pH. We hypothesized that the cells used the Cl⁻/HCO₃⁻ exchanger to export the HCO₃⁻ ions outside the cells and thus maintain a pH_i level close to the physiological one.

cell lines is necessary for optimal Na⁺/H⁺ exchange [21,83–85]. As already seen, U87 cells were able to reduce intracellular acidity by Na⁺/H⁺ exchange over 8 hours. The exchanger operated normally during this period. Assuming that the activity of a NHE exchanger in U87 cells depends on the availability of intracellular ATP, the NHE exchanger might have exhausted the intracellular ATP necessary for the various mitochondrial functions, in particular for maintaining the membrane potential gradient which stimulates cell survival and proliferation [86,87]. The depletion of ATP by the NHE exchanger therefore leads to cell death this could explain the higher mortality of U87 cells compared to F98 cells.

Very few studies have been conducted to investigate the effect of alkaline pH_e on cell survival [88–92]. These studies did not focus on the study of cellular metabolism but rather on the effect of extracellular alkalinization on the permeability of the plasma membrane [88,91,92]. It was found that the morphology of cells was altered in alkalinized culture. The spindle-shaped cells, like F98 cells, formed small patches of round cells at basic pH_e [92]. Moreover, the cells had lost their ability to adhesion. Consequently, the membrane potential of mitochondria was altered leading to permeability transition, pore opening, and thus cell death [93,94]. Cells that grow as cell aggregates such as U87 cells, are therefore

more resistant to cell death under basic pH_e .

Conclusion and future work

Many cellular processes and therapeutic agents are known to be highly pH-dependent, making the study of intracellular pH (pH_i) regulation of utmost importance. Therefore, this study made it possible to focus on the regulation of the pH_i of two brain tumor cells using fluorescence microscopy. We observed that the tumor regulation of acidity is not the same for the two cell lines and as a consequence, our results do not support the common idea that tumor cells behave in a similarly way. On the other hand, pH_i regulation appears highly cell-dependent.

In order to interpret our results, we have proposed hypotheses to explain the mechanisms involved in the regulation of pH_i . In 2D monolayer cultures, we assumed that F98 rat glioma cells do not regulate intracellular acidity, preserve protons inside the cells by activating the V-ATPase pump at acidic pH to bring H^+ ions into lysosomes. The study of the effect of the inhibition of the V-ATPase pump, by bafilomycin A1 [95], on the pH_i would be an excellent tool to validate our interpretation. On the other hand, we hypothesized that human glioblastoma U87 cells, that are found to regulate intracellular acidity, use the Na^+/H^+ exchanger to export H^+ ions outside the cells. Therefore, testing amiloride as a Na^+/H^+ exchanger inhibitor [96] can be an effective tool to validate our hypothesis.

In addition, in order to properly characterize the tumor regulation of pH_i , it is crucial to study it at the scale of a spheroid. This 3D model constitute an intermediate biological model between 2D cell cultures and animal models and develop a relationship between the cells and their heterogeneous environment characterized by substrates fluxes and gradients. More precisely, cells growing in a spheroid are exposed not only to reduced pH_e levels, as 2D monolayer cultures, but also to a limitation of the supply of nutrients and oxygen, due to their diffusion inside the spheroid. Differences in results between 2D and 3D experiments were therefore expected. Tidwell *et al.*, 2022 [97] have recently shown that the combination of hypoxia, starvation of other nutrients and extracellular acidity inhibit energy metabolism or protein synthesis and prevent the regulation of exchanges such as Na^+/H^+ in 3D spheroids. This is in a great agreement with the results obtained on the U87 spheroids: contrary to the results obtained in 2D monolayer cultures, the fact that the U87 spheroids lowered their pH_i under acidic conditions can be explained by the inhibition of the Na^+/H^+ exchanger.

The effect of Tomozolomide (TMZ), the cornerstone drug used against brain tumors, is highly pH-dependent [98]. Since tumor cells can acidify their microenvironment and regulate their intracellular pH, this may influence the efficacy of TMZ. A recent theoretical study has shown that the pH_i regulation capacity of a cell line can be exploited to estimate the optimum pH_e for TMZ efficacy [35]. Therefore, the effect of TMZ was studied on our two cell lines by manipulating the extracellular pH (pH_e). The results has allowed us to show that drug efficiency depend on the cell type and on the pH_e , which gives an argument for considering pH as a personalized therapeutic target for future research based on the combination of TMZ with pH-regulating agents.

Author Contributions: Data curation, Arnold Fertin; Formal analysis, Pierre Jacquet; Funding acquisition, Angélique Stéphanou; Investigation, Alaa Tafech; Methodology, Arnold Fertin, Yves Usson and Angélique Stéphanou; Resources, Céline Beaujean; Software, Pierre Jacquet and Arnold Fertin; Supervision, Angélique Stéphanou; Writing – original draft, Alaa Tafech; Writing – review & editing, Angélique Stéphanou.

Funding: This project has received financial support from the CNRS through the MITI interdisciplinary programs (MetaMod Project 2021-2022). We are very grateful to Annabelle Ballesta (Institut Curie) and Olivier Seksek (IJCLab) for their advices and helpful discussions.

Institutional Review Board Statement: Not applicable.

Informed Consent Statement: Not applicable.

Data Availability Statement: Not applicable

Conflicts of Interest: The authors declare no conflict of interest.

Appendix A

The full methodology to identify the optimum wavelengths for pH measurements is described in full details in Tafech *et al.*, 2023 [41]. In this appendix we present the emission spectra of the intracellular BCECF probe obtained for the two cell lines at various pH values of the calibration DMEM solution, ranging from pH 4 to 9 (Fig. A1). A double excitation at 405 nm and 488 nm is used.

Based on the principle of the ratiometric method, a combination of two remarkable emission wavelengths allow to evaluate the intracellular pH as a function of the ratio of fluorescence intensities. In this context, all the combinations that can be made between two given remarkable emission wavelength were analyzed. For each cell line, the analyzed combinations are shown in figure A2. For each combination, the ratio of fluorescence intensities measured at the two remarkable emission wavelengths is monitored as a function of pH and the curve $R = f(\text{pH}_i)$ is thus constructed. As in the methodological paper [41] that considered the extracellular BCECF probe, two types of regression (linear and polynomial) were used to estimate the relationship between the pH_i and the fluorescence ratio in order to find the best-fit line that best expresses the relationship between the data points. A percent error δ was also calculated to evaluate the importance of the difference between the pH_i value effectively measured and the reference value.

We have found that the best method to measure the intracellular pH of F98 cells is to set the emission wavelength at 517 nm for the 405 nm laser and 546 nm for the 488 nm laser. In this case the pH is monitored as a function of the fluorescence ratio $R = I_{517\text{nm}} / I_{546\text{nm}}$. Whereas for U87 cells, the intracellular pH is measured by fixing the emission wavelength at 556 nm for the 405 nm laser and at 517 nm for the 488 nm laser. In this case the pH is monitored as a function of the fluorescence ratio $R = I_{517\text{nm}} / I_{556\text{nm}}$. The calibration curves obtained for pH_i measurements for the two cell lines are given in figure A3.

References

- Vaupel, P.; Kallinowski, F.; Okunieff, P. Blood flow, oxygen and nutrient supply, and metabolic microenvironment of human tumors: a review. *Cancer research* **1989**, *49*, 6449–6465.
- Kallinowski, F.; Vaupel, P. pH distributions in spontaneous and isografted rat tumours. *British Journal of Cancer* **1988**, *58*, 314–321. <https://doi.org/10.1038/bjc.1988.210>.
- Chiche, J.; Brahim-Horn, M.C.; Pouyssegur, J. Tumour hypoxia induces a metabolic shift causing acidosis: a common feature in cancer. *Journal of Cellular and Molecular Medicine* **2010**, *14*, 771–794. <https://doi.org/10.1111/j.1582-4934.2009.00994.x>.
- Smallbone, K.; Gavaghan, D.J.; Gatenby, R.A.; Maini, P.K. The role of acidity in solid tumour growth and invasion. *Journal of Theoretical Biology* **2005**, *235*, 476–484. <https://doi.org/10.1016/j.jtbi.2005.02.001>.
- Justus, C.R.; Dong, L.; Yang, L.V. Acidic tumor microenvironment and pH-sensing G protein-coupled receptors. *Frontiers in Physiology* **2013**, *4*. <https://doi.org/10.3389/fphys.2013.00354>.
- Parks, S.K.; Cormerais, Y.; Pouyssegur, J. Hypoxia and cellular metabolism in tumour pathophysiology. *The Journal of Physiology* **2017**, *595*, 2439–2450. <https://doi.org/10.1113/jp273309>.
- Druzhkova, I.; Shirmanova, M.; Lukina, M.; Dudenkova, V.; Sergeeva, T.; Belousov, V.; Lukyanov, S.; Zagaynova, E. Registration of intracellular pH in cancer cells with genetically encoded ratiometric sensor, 2015. <https://doi.org/10.1364/ecbo.2015.953710>.
- Shirmanova, M.V.; Druzhkova, I.N.; Lukina, M.M.; Matlashov, M.E.; Belousov, V.V.; Snopova, L.B.; Prodanetz, N.N.; Dudenkova, V.V.; Lukyanov, S.A.; Zagaynova, E.V. Intracellular pH imaging in cancer cells in vitro and tumors in vivo using the new

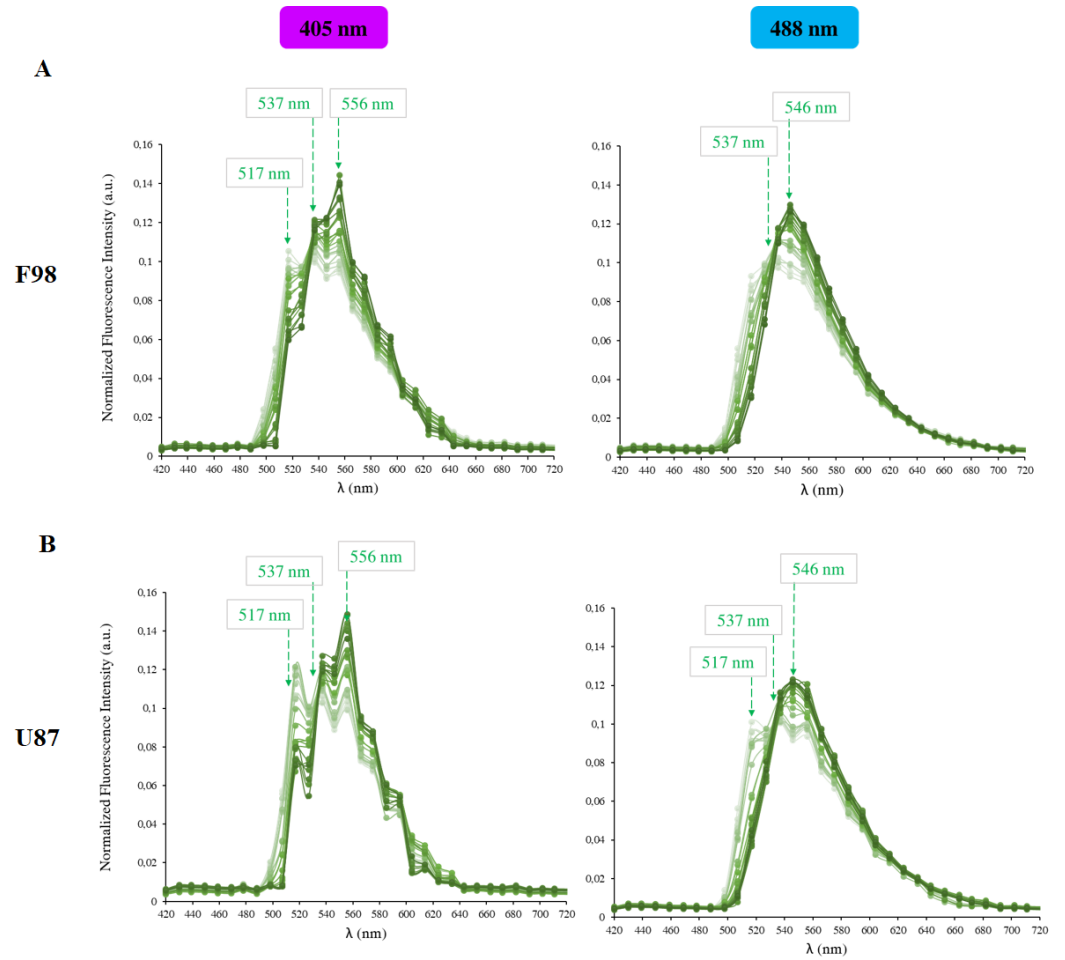


Figure A1. BCECF ($5\mu\text{M}$) emission spectra at 405 nm (left), 488 nm (right) excitation wavelengths, in (a) F98 and (b) U87 at various pH values. The remarkable emission wavelengths taken for the ratiometric measurements are designated by arrows.

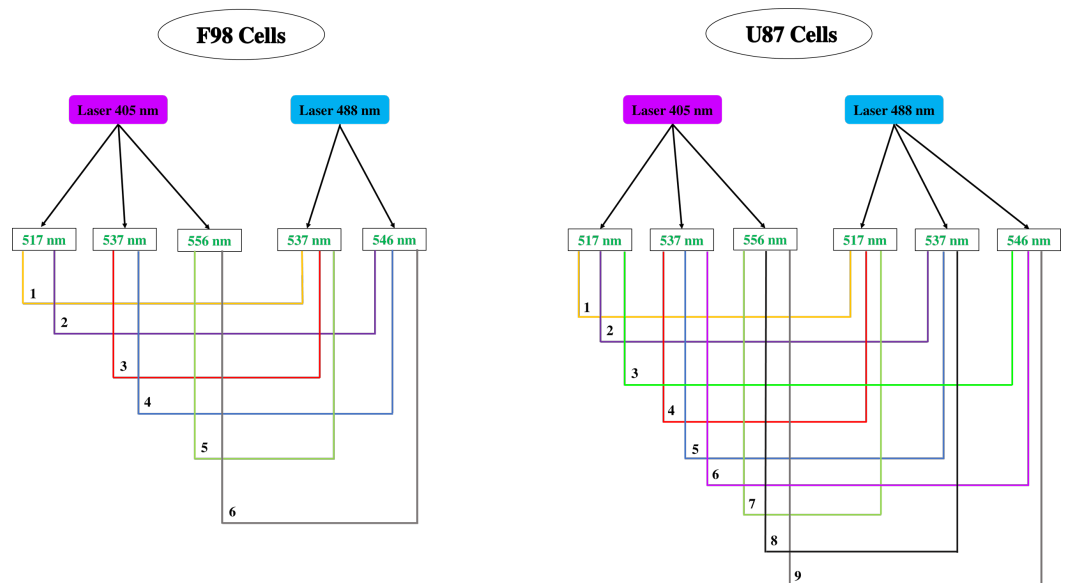


Figure A2. The combinations made, for each cell line, between two remarkable emission wavelengths noted on the emission spectra of the permeable version of the BCECF (BCECF-AM). For each combination, the ratio of fluorescence intensities measured at the two remarkable emission wavelengths is monitored as a function of pH.

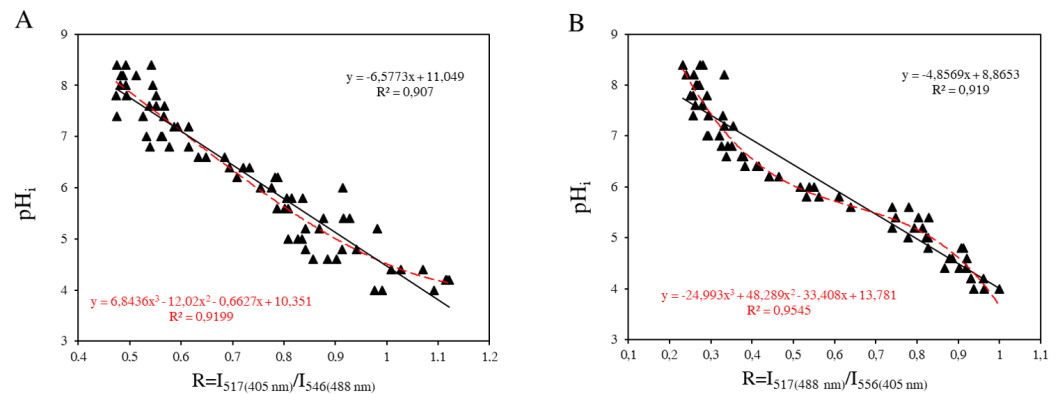


Figure A3. Calibration curves for intracellular pH measurements with the internalized BCECF probe for F98 cells (A) and U87 cells (B) (data set in triplicate).

- genetically encoded sensor SypHer2. *Biochimica et Biophysica Acta (BBA) - General Subjects* **2015**, *1850*, 1905–1911. <https://doi.org/10.1016/j.bbagen.2015.05.001>. 808
9. Gillies, R.J.; Raghunand, N.; Karczmar, G.S.; Bhujwala, Z.M. MRI of the tumor microenvironment. *Journal of Magnetic Resonance Imaging* **2002**, *16*, 430–450. <https://doi.org/10.1002/jmri.10181>. 809
 10. Roos, A.; Boron, W.F. Intracellular pH. *Physiological Reviews* **1981**, *61*, 296–434. <https://doi.org/10.1152/physrev.1981.61.2.296>. 810
 11. Madshus, I.H. Regulation of intracellular pH in eukaryotic cells. *Biochemical Journal* **1988**, *250*, 1–8. <https://doi.org/10.1042/bj2500001>. 811
 12. Zhuang, Y.X.; Cragoe, E.J.; Shaikewitz, T.; Glaser, L.; Cassel, D. Characterization of potent sodium/proton exchange inhibitors from the amiloride series in A431 cells. *Biochemistry* **1984**, *23*, 4481–4488. <https://doi.org/10.1021/bi00314a038>. 812
 13. Barathova, M.; Takacova, M.; Holotnakova, T.; Gibadulinova, A.; Ohradanova, A.; Zatovicova, M.; Hulikova, A.; Kopacek, J.; Parkkila, S.; Supuran, C.T.; et al. Alternative splicing variant of the hypoxia marker carbonic anhydrase IX expressed independently of hypoxia and tumour phenotype. *British Journal of Cancer* **2007**, *98*, 129–136. <https://doi.org/10.1038/sj.bjc.6604111>. 813
 14. Hinton, A.; Sennoune, S.R.; Bond, S.; Fang, M.; Reuveni, M.; Sahagian, G.G.; Jay, D.; Martinez-Zaguilan, R.; Forgac, M. Function of a Subunit Isoforms of the V-ATPase in pH Homeostasis and in Vitro Invasion of MDA-MB231 Human Breast Cancer Cells. *Journal of Biological Chemistry* **2009**, *284*, 16400–16408. <https://doi.org/10.1074/jbc.m901201200>. 814
 15. Enerson, B.E.; Drewes, L.R. Molecular Features, Regulation, and Function of Monocarboxylate Transporters: Implications for Drug Delivery. *Journal of Pharmaceutical Sciences* **2003**, *92*, 1531–1544. <https://doi.org/10.1002/jps.10389>. 815
 16. Supuran, C.T.; Fiore, A.D.; Alterio, V.; Montib, S.M.; Simone, G.D. Recent Advances in Structural Studies of the Carbonic Anhydrase Family: The Crystal Structure of Human CA IX and CA XIII. *Current Pharmaceutical Design* **2010**, *16*, 3246–3254. <https://doi.org/10.2174/138161210793429841>. 816
 17. Pouyssegur, J.; Dayan, F.; Mazure, N.M. Hypoxia signalling in cancer and approaches to enforce tumour regression. *Nature* **2006**, *441*, 437–443. <https://doi.org/10.1038/nature04871>. 817
 18. Sennoune, S.R.; Bakunts, K.; Martínez, G.M.; Chua-Tuan, J.L.; Kebir, Y.; Attaya, M.N.; Martínez-Zaguilán, R. Vacuolar Hsup/sup-ATPase in human breast cancer cells with distinct metastatic potential: distribution and functional activity. *American Journal of Physiology-Cell Physiology* **2004**, *286*, C1443–C1452. <https://doi.org/10.1152/ajpcell.00407.2003>. 818
 19. Montcourrier, P.; Silver, I.; Farnoud, R.; Bird, I.; Rochefort, H. *Clinical and Experimental Metastasis* **1997**, *15*, 382–392. <https://doi.org/10.1023/a:1018446104071>. 819
 20. Grillon, E.; Farion, R.; Fablet, K.; Waard, M.D.; Tse, C.M.; Donowitz, M.; Rémy, C.; Coles, J.A. The Spatial Organization of Proton and Lactate Transport in a Rat Brain Tumor. *PLoS ONE* **2011**, *6*, e17416. <https://doi.org/10.1371/journal.pone.0017416>. 820
 21. Kapus, A.; Grinstein, S.; Wasan, S.; Kandasamy, R.; Orłowski, J. Functional characterization of three isoforms of the Na/H exchanger stably expressed in Chinese hamster ovary cells. ATP dependence, osmotic sensitivity, and role in cell proliferation. *Journal of Biological Chemistry* **1994**, *269*, 23544–23552. [https://doi.org/10.1016/s0021-9258\(17\)31550-8](https://doi.org/10.1016/s0021-9258(17)31550-8). 821
 22. Pouyssegur, J.; Chambard, J.C.; Franchi, A.; Paris, S.; Obberghen-Schilling, E.V. Growth factor activation of an amiloride-sensitive Na/H exchange system in quiescent fibroblasts: coupling to ribosomal protein S6 phosphorylation. *Proceedings of the National Academy of Sciences* **1982**, *79*, 3935–3939. <https://doi.org/10.1073/pnas.79.13.3935>. 822
 23. Denker, S.P.; Huang, D.C.; Orłowski, J.; Furthmayr, H.; Barber, D.L. Direct Binding of the Na–H Exchanger NHE1 to ERM Proteins Regulates the Cortical Cytoskeleton and Cell Shape Independently of H Translocation. *Molecular Cell* **2000**, *6*, 1425–1436. [https://doi.org/10.1016/s1097-2765\(00\)00139-8](https://doi.org/10.1016/s1097-2765(00)00139-8). 823
 24. Turchi, L.; Loubat, A.; Rochet, N.; Rossi, B.; Ponzio, G. Evidence for a Direct Correlation between c-Jun NH2 Terminal Kinase 1 Activation, Cyclin D2 Expression, and G1/S Phase Transition in the Murine Hybridoma 7TD1 Cells. *Experimental Cell Research* **2000**, *261*, 220–228. <https://doi.org/10.1006/excr.2000.5060>. 824

25. Putney, L.K.; Barber, D.L. Na-H Exchange-dependent Increase in Intracellular pH Times G2/M Entry and Transition. *Journal of Biological Chemistry* **2003**, *278*, 44645–44649. <https://doi.org/10.1074/jbc.m308099200>. 850
26. Uzman, J.; Patil, S.; Uzgare, A.R.; Sater, A.K. The Role of Intracellular Alkalinization in the Establishment of Anterior Neural Fate in *Xenopus*. *Developmental Biology* **1998**, *193*, 10–20. <https://doi.org/10.1006/dbio.1997.8782>. 851
27. Boussouf, A.; Gaillard, S. Intracellular pH changes during oligodendrocyte differentiation in primary culture. *Journal of Neuroscience Research* **2000**, *59*, 731–739. [https://doi.org/10.1002/\(sici\)1097-4547\(20000315\)59:6<731::aid-jnr5>3.0.co;2-g](https://doi.org/10.1002/(sici)1097-4547(20000315)59:6<731::aid-jnr5>3.0.co;2-g). 852
28. Sharma, M.; Astekar, M.; Soi, S.; Manjunatha, B.; Shetty, D.; Radhakrishnan, R. pH Gradient Reversal: An Emerging Hallmark of Cancers. *Recent Patents on Anti-Cancer Drug Discovery* **2015**, *10*, 244–258. <https://doi.org/10.2174/1574892810666150708110608>. 853
29. Brophy, G.T.; Sladek, N. Influence of pH on the cytotoxic activity of chlorambucil. *Biochemical Pharmacology* **1983**, *32*, 79–84. [https://doi.org/10.1016/0006-2952\(83\)90656-1](https://doi.org/10.1016/0006-2952(83)90656-1). 854
30. Skarsgard, L.D.; Skwarchuk, M.W.; Vinczan, A.; Kristl, J.; Chaplin, D.J. The cytotoxicity of melphalan and its relationship to pH, hypoxia and drug uptake. *Anticancer research* **1995**, *15*, 219–223. 855
31. Born, R.; Eichholtz-Wirth, H. Effect of different physiological conditions on the action of adriamycin on Chinese hamster cells in vitro. *British Journal of Cancer* **1981**, *44*, 241–246. <https://doi.org/10.1038/bjc.1981.175>. 856
32. Hindenburg, A.A.; Gervasoni, J.E.; Krishna, S.; Stewart, V.J.; Rosado, M.; Lutzky, J.; Bhalla, K.; Baker, M.A.; Taub, R.N. Intracellular distribution and pharmacokinetics of daunorubicin in anthracycline-sensitive and -resistant HL-60 cells. *Cancer research* **1989**, *49*, 4607–4614. 857
33. Jähde, E.; Glüsenkamp, K.H.; Rajewsky, M.F. Protection of cultured malignant cells from mitoxantrone cytotoxicity by low extracellular pH: A possible mechanism for chemoresistance in vivo. *European Journal of Cancer and Clinical Oncology* **1990**, *26*, 101–106. [https://doi.org/10.1016/0277-5379\(90\)90290-a](https://doi.org/10.1016/0277-5379(90)90290-a). 858
34. Vukovic, V.; Tannock, I. Influence of low pH on cytotoxicity of paclitaxel, mitoxantrone and topotecan. *British Journal of Cancer* **1997**, *75*, 1167–1172. <https://doi.org/10.1038/bjc.1997.201>. 859
35. Stéphanou, A.; Ballesta, A. pH as a potential therapeutic target to improve temozolomide antitumor efficacy : A mechanistic modeling study. *Pharmacology Research and Perspectives* **2019**, *7*, e00454. <https://doi.org/10.1002/prp2.454>. 860
36. Andersen, A.P.; Moreira, J.M.A.; Pedersen, S.F. Interactions of ion transporters and channels with cancer cell metabolism and the tumour microenvironment. *Philosophical Transactions of the Royal Society B* **2014**, *369*, 20130098. <https://doi.org/10.1098/rstb.2013.0098>. 861
37. Parks, S.K.; Chiche, J.; Pouysségur, J. Disrupting proton dynamics and energy metabolism for cancer therapy. *Nature Reviews Cancer* **2013**. 862
38. Neri, D.; Supuran, C.T. Interfering with pH regulation in tumours as a therapeutic strategy. *Nature Reviews drug discovery* **2011**, *10*, 767–777. <https://doi.org/10.1038/nrd3554>. 863
39. Lee, E.S.; Gao, Z.; Bae, Y.H. Recent progress in tumor pH targeting nanotechnology. *Journal of controlled release : official journal of the Controlled Release Society* **2008**, *132*, 164–170. <https://doi.org/10.1016/j.jconrel.2008.05.003>. 864
40. Song, S.; Chen, F.; Qi, H.; Li, F.; Xin, T.; Xu, J.; Ye, T.; Sheng, N.; Yang, X.; Pan, W. Multifunctional Tumor-Targeting Nanocarriers Based on Hyaluronic Acid-Mediated and pH-Sensitive Properties for Efficient Delivery of Docetaxel. *Pharmaceutical Research* **2014**, *31*, 1032–1045. <https://doi.org/10.1007/s11095-013-1225-y>. 865
41. Tafech, A.; Beaujean, C.; Usson, Y.; Stéphanou, A. Generalization of the ratiometric method to extend pH range measurements of the BCECF probe. *Biomolecules* **2023**, *13*, 442. <https://doi.org/10.3390/biom13030442>. 866
42. Oraiopoulou, M.E.; Tzamali, E.; Tzedakis, G.; Vakis, A.; Papamatheakis, J.; Sakkalis, V. In Vitro/In Silico Study on the Role of Doubling Time Heterogeneity among Primary Glioblastoma Cell Lines. *BioMed Research International* **2017**, *2017*, 1–12. <https://doi.org/10.1155/2017/8569328>. 867
43. Mathews, M.S.; Blickenstaff, J.W.; Shih, E.C.; Zamora, G.; Vo, V.; Sun, C.H.; Hirschberg, H.; Madsen, S.J. Photochemical internalization of bleomycin for glioma treatment. *Journal of Biomedical Optics* **2012**, *17*, 058001. <https://doi.org/10.1117/1.jbo.17.5.058001>. 868
44. Tsien, R.Y. A non-disruptive technique for loading calcium buffers and indicators into cells. *Nature* **1981**, *290*, 527–528. <https://doi.org/10.1038/290527a0>. 869
45. Graber, M.L.; DiLillo, D.C.; Friedman, B.L.; Pastoriza-Munoz, E. Characteristics of fluoroprobes for measuring intracellular pH. *Analytical Biochemistry* **1986**, *156*, 202–212. [https://doi.org/10.1016/0003-2697\(86\)90174-0](https://doi.org/10.1016/0003-2697(86)90174-0). 870
46. Damaghi, M.; Wojtkowiak, J.W.; Gillies, R.J. pH sensing and regulation in cancer. *Frontiers in Physiology* **2013**, *4*. <https://doi.org/10.3389/fphys.2013.00370>. 871
47. Izutsu, K.T. Intracellular pH, H ion flux and H ion permeability coefficient in bullfrog toe muscle. *The Journal of Physiology* **1972**, *221*, 15–27. <https://doi.org/10.1113/jphysiol.1972.sp009735>. 872
48. Baltz, J.; Biggers, J.; Lechene, C. A novel H permeability dominating intracellular pH in the early mouse embryo. *Development* **1993**, *118*, 1353–1361. <https://doi.org/10.1242/dev.118.4.1353>. 873
49. Doyen, D.; Poët, M.; Jarretou, G.; Pisani, D.F.; Tauc, M.; Coughon, M.; Argentina, M.; Bouret, Y.; Counillon, L. Intracellular pH Control by Membrane Transport in Mammalian Cells. Insights Into the Selective Advantages of Functional Redundancy. *Frontiers in Molecular Biosciences* **2022**, *9*. <https://doi.org/10.3389/fmolb.2022.825028>. 874

50. Carmelo, V.; Santos, H.; Sá-Correia, I. Effect of extracellular acidification on the activity of plasma membrane ATPase and on the cytosolic and vacuolar pH of *Saccharomyces cerevisiae*. *Biochimica et Biophysica Acta (BBA) - Biomembranes* **1997**, *1325*, 63–70. [https://doi.org/10.1016/s0005-2736\(96\)00245-3](https://doi.org/10.1016/s0005-2736(96)00245-3).
51. Glunde, K.; Dussmann, H.; Juretschke, H.P.; Leibfritz, D. Na/H exchange subtype 1 inhibition during extracellular acidification and hypoxia in glioma cells. *Journal of Neurochemistry* **2002**, *80*, 36–44. <https://doi.org/10.1046/j.0022-3042.2001.00661.x>.
52. Lacoste, I.; Harvey, B.; Ehrenfeld, J. Cl⁻ permeability of the basolateral membrane of the *Rana esculenta* epithelium: activation of Cl⁻/HCO₃⁻ exchange by alkaline intracellular pH. *Biochimica et Biophysica Acta (BBA) - Biomembranes* **1991**, *1063*, 103–110. [https://doi.org/10.1016/0005-2736\(91\)90359-g](https://doi.org/10.1016/0005-2736(91)90359-g).
53. Vilariño, N.; Vieytes, M.R.; Vieites, J.M.; Botana, L.M. Role of HCO₃⁻ ions in Cytosolic pH Regulation in Rat Mast Cells: Evidence for a New Na-Independent, HCO₃⁻-Dependent Alkalinizing Mechanism. *Biochemical and Biophysical Research Communications* **1998**, *253*, 320–324. <https://doi.org/10.1006/bbrc.1998.9615>.
54. Rivarola, V.; Ford, P.; Chara, O.; Parisi, M.; Capurro, C. Functional and Molecular Adaptation of Cl⁻/HCO₃⁻ Exchanger to Chronic Alkaline Media in Renal Cells. *Cellular Physiology and Biochemistry* **2005**, *16*, 271–280. <https://doi.org/10.1159/000089853>.
55. Swietach, P.; Vaughan-Jones, R.D.; Harris, A.L.; Hulikova, A. The chemistry, physiology and pathology of pH in cancer. *Philosophical Transactions of the Royal Society B: Biological Sciences* **2014**, *369*, 20130099. <https://doi.org/10.1098/rstb.2013.0099>.
56. Estrella, V.; Chen, T.; Lloyd, M.; Wojtkowiak, J.; Cornnell, H.H.; Ibrahim-Hashim, A.; Bailey, K.; Balagurunathan, Y.; Rothberg, J.M.; Sloane, B.F.; et al. Acidity Generated by the Tumor Microenvironment Drives Local Invasion. *Cancer Research* **2013**, *73*, 1524–1535. <https://doi.org/10.1158/0008-5472.can-12-2796>.
57. Corbet, C.; Feron, O. Tumour acidosis: from the passenger to the driver's seat. *Nature Reviews Cancer* **2017**, *17*, 577–593. <https://doi.org/10.1038/nrc.2017.77>.
58. Hackam, D.J.; Grinstein, S.; Rotstein, O.D. Intracellular pH regulation in leukocytes. *Shock* **1996**, *5*, 17–21. <https://doi.org/10.1097/00024382-199601000-00005>.
59. Rao, M.; Streur, T.L.; Aldwell, F.E.; Cook, G.M. Intracellular pH regulation by *Mycobacterium smegmatis* and *Mycobacterium bovis* BCG. *Microbiology* **2001**, *147*, 1017–1024. <https://doi.org/10.1099/00221287-147-4-1017>.
60. Zeng, W.P.; Yang, S.; Zhou, B. Intracellular pH-regulated Cell Intrinsic Control of Death and Proliferation of Lymphocytes in Immune Response and Tumor Cells. *BioRxiv* **2021**. <https://doi.org/10.1101/2021.10.29.466539>.
61. Man, C.H.; Mercier, F.E.; Liu, N.; Dong, W.; Stephanopoulos, G.; Jiang, L.; Jung, Y.; Lin, C.P.; Leung, A.Y.H.; Scadden, D.T. Proton export alkalinizes intracellular pH and reprograms carbon metabolism to drive normal and malignant cell growth. *Blood* **2022**, *139*, 502–522. <https://doi.org/10.1182/blood.2021011563>.
62. Hirschhaeuser, F.; Menne, H.; Dittfeld, C.; West, J.; Mueller-Klieser, W.; Kunz-Schughart, L.A. Multicellular tumor spheroids: An underestimated tool is catching up again. *Journal of Biotechnology* **2010**, *148*, 3–15. <https://doi.org/10.1016/j.jbiotec.2010.01.012>.
63. Freyer, J.P.; Sutherland, R.M. A reduction in the in situ rates of oxygen and glucose consumption of cells in EMT6/Ro spheroids during growth. *Journal of Cellular Physiology* **1985**, *124*, 516–524. <https://doi.org/10.1002/jcp.1041240323>.
64. Sutherland, R.M. Cell and Environment Interactions in Tumor Microregions: The Multicell Spheroid Model. *Science* **1988**, *240*, 177–184. <https://doi.org/10.1126/science.2451290>.
65. Friedrich, J.; Seidel, C.; Ebner, R.; Kunz-Schughart, L.A. Spheroid-based drug screen: considerations and practical approach. *Nature Protocols* **2009**, *4*, 309–324. <https://doi.org/10.1038/nprot.2008.226>.
66. Murphy, K.C.; Hung, B.P.; Browne-Bourne, S.; Zhou, D.; Yeung, J.; Genetos, D.C.; Leach, J.K. Measurement of oxygen tension within mesenchymal stem cell spheroids. *Journal of The Royal Society Interface* **2017**, *14*, 20160851. <https://doi.org/10.1098/rsif.2016.0851>.
67. Galkina, S.; Sud'ina, G.; Margolis, L. Regulation of intracellular pH by phospholipase A2 and protein kinase C upon neutrophil adhesion to solid substrata. *FEBS Letters* **1996**, *393*, 117–120. [https://doi.org/10.1016/0014-5793\(96\)00864-2](https://doi.org/10.1016/0014-5793(96)00864-2).
68. Galkina, S.; Sud'ina, G.; Dergacheva, G.; Margolis, L. Regulation of intracellular pH by cell-cell adhesive interactions. *FEBS Letters* **1995**, *374*, 17–20. [https://doi.org/10.1016/0014-5793\(95\)00969-g](https://doi.org/10.1016/0014-5793(95)00969-g).
69. Zagaynova, E.V.; Druzhkova, I.N.; Mishina, N.M.; Ignatova, N.I.; Dudenkova, V.V.; Shirmanova, M.V. Imaging of Intracellular pH in Tumor Spheroids Using Genetically Encoded Sensor SypHer2. In *Advances in Experimental Medicine and Biology*; Springer International Publishing, 2017; pp. 105–119. https://doi.org/10.1007/978-3-319-67358-5_7.
70. Ballesta, A.; Zhou, Q.; Zhang, X.; Lv, H.; Gallo, J. Multiscale Design of Cell-Type-Specific Pharmacokinetic/Pharmacodynamic Models for Personalized Medicine: Application to Temozolomide in Brain Tumors. *CPT: Pharmacometrics & Systems Pharmacology* **2014**, *3*, 112. <https://doi.org/10.1038/psp.2014.9>.
71. Gnochì, D.; Sabbà, C.; Mazzocca, A. Lactic acid fermentation: a maladaptative mechanism and an evolutionary throwback boosting cancer drug resistance. *Biochimie* **2023**.
72. Gnochì, D.; Nikolic, D.; Paparella, R.R.; Sabbà, C.; Mazzocca, A. Cellular adaptation take advantage of atavistic regression programs during carcinogenesis. *Cancers* **2023**.
73. Jacquet, P.; Stéphanou, A. Metabolic Reprogramming, Questioning, and Implications for Cancer. *Biology* **2021**, *10*. <https://doi.org/10.3390/biology10020129>.
74. Jacquet, P.; Stéphanou, A. Searching for the metabolic signature of cancer: a review from Warburg's time to now. *Biomolecules* **2022**, *12*, 1412. <https://doi.org/10.3390/biom12101412>.

75. Jacquet, P.; Stéphanou, A. A reduced model of cell metabolism to revisit the glycolysis-OXPHOS relationship in the deregulated tumor microenvironment. *J theor Biol* **2023**, *562*, 111434. <https://doi.org/10.1016/j.jtbi.2023.111434>. 966
76. Tannock, I.F.; Rotin, D. Acid pH in tumors and its potential for therapeutic exploitation. *Cancer research* **1989**, *49*, 16, 4373–84. 967
77. Wahl, M.L.; Pooler, P.M.; Briand, P.; Leeper, D.B.; Owen, C.S. Intracellular pH regulation in a nonmalignant and a derived malignant human breast cell line. *Journal of Cellular Physiology* **2000**, *183*, 373–380. [https://doi.org/10.1002/\(sici\)1097-4652\(200006\)183:3<373::aid-jcp10>3.0.co;2-s](https://doi.org/10.1002/(sici)1097-4652(200006)183:3<373::aid-jcp10>3.0.co;2-s). 968
78. Piao, S.; Amaravadi, R.K. Targeting the lysosome in cancer. *Annals of the New York Academy of Sciences* **2015**, *1371*, 45–54. <https://doi.org/10.1111/nyas.12953>. 969
79. Tang, T.; Yu Yang, Z.; Wang, D.; Yan Yang, X.; Wang, J.; Li, L.; Wen, Q.; Gao, L.; Wu Bian, X.; Cang Yu, S. The role of lysosomes in cancer development and progression. *Cell & Bioscience* **2020**, *10*. <https://doi.org/10.1186/s13578-020-00489-x>. 970
80. Chen, R.; Jäättelä, M.; Liu, B. Lysosome as a Central Hub for Rewiring PH Homeostasis in Tumors. *Cancers* **2020**, *12*, 2437. <https://doi.org/10.3390/cancers12092437>. 971
81. Banerjee, S.; Kane, P.M. Regulation of V-ATPase Activity and Organelle pH by Phosphatidylinositol Phosphate Lipids. *Frontiers in Cell and Developmental Biology* **2020**, *8*. <https://doi.org/10.3389/fcell.2020.00510>. 972
82. Kinsella, J.L.; Aronson, P.S. Properties of the Na-H exchanger in renal microvillus membrane vesicles. *American Journal of Physiology-Renal Physiology* **1980**, *238*, F461–F469. <https://doi.org/10.1152/ajprenal.1980.238.6.f461>. 973
83. Cassel, D.; Katz, M.; Rotman, M. Depletion of cellular ATP inhibits Na/H antiport in cultured human cells. Modulation of the regulatory effect of intracellular protons on the antiporter activity. *Journal of Biological Chemistry* **1986**, *261*, 5460–5466. [https://doi.org/10.1016/s0021-9258\(19\)57238-6](https://doi.org/10.1016/s0021-9258(19)57238-6). 974
84. Brown, S.E.; Heming, T.A.; Benedict, C.R.; Bidani, A. ATP-sensitive Na⁽⁺⁾-H antiport in type II alveolar epithelial cells. *American Journal of Physiology-Cell Physiology* **1991**, *261*, C954–C963. <https://doi.org/10.1152/ajpcell.1991.261.6.c954>. 975
85. Levine, S.A.; Montrose, M.H.; Tse, C.M.; Donowitz, M. Kinetics and regulation of three cloned mammalian Na⁺/H⁺ exchangers stably expressed in a fibroblast cell line. *The Journal of Biological Chemistry* **1993**, *268*, 25527–25535. [https://doi.org/10.1016/s0021-9258\(19\)74423-8](https://doi.org/10.1016/s0021-9258(19)74423-8). 976
86. Brown, S.V.; Hosking, P.; Li, J.; Williams, N. ATP Synthase Is Responsible for Maintaining Mitochondrial Membrane Potential in Bloodstream Form *i*Trypanosoma brucei/*i*. *Eukaryotic Cell* **2006**, *5*, 45–53. <https://doi.org/10.1128/ec.5.1.45-53.2006>. 977
87. Vasan, K.; Clutter, M.; Dunne, S.F.; George, M.D.; Luan, C.H.; Chandel, N.S.; Martínez-Reyes, I. Genes Involved in Maintaining Mitochondrial Membrane Potential Upon Electron Transport Chain Disruption. *Frontiers in Cell and Developmental Biology* **2022**, *10*. <https://doi.org/10.3389/fcell.2022.781558>. 978
88. Langer, G.A. The effect of pH on cellular and membrane calcium binding and contraction of myocardium. A possible role for sarcolemmal phospholipid in EC coupling. *Circulation Research* **1985**, *57*, 374–382. <https://doi.org/10.1161/01.res.57.3.374>. 979
89. Wanandi, S.; Yustisia, I.; Neolaka, G.; Jusman, S. Impact of extracellular alkalization on the survival of human CD24⁺/CD44⁺ breast cancer stem cells associated with cellular metabolic shifts. *Brazilian Journal of Medical and Biological Research* **2017**, *50*. <https://doi.org/10.1590/1414-431x20176538>. 980
90. Khajah, M.A.; Almohri, I.; Mathew, P.M.; Luqmani, Y.A. Extracellular Alkaline pH Leads to Increased Metastatic Potential of Estrogen Receptor Silenced Endocrine Resistant Breast Cancer Cells. *PLoS ONE* **2013**, *8*, e76327. <https://doi.org/10.1371/journal.pone.0076327>. 981
91. Avnet, S.; Lemma, S.; Cortini, M.; Pellegrini, P.; Perut, F.; Zini, N.; Kusuzaki, K.; Chano, T.; Grisendi, G.; Dominici, M.; et al. Altered pH gradient at the plasma membrane of osteosarcoma cells is a key mechanism of drug resistance. *Oncotarget* **2016**, *7*, 63408–63423. <https://doi.org/10.18632/oncotarget.11503>. 982
92. Güvenalp, N.; Güvenç, D. An evaluation of the effects of medium pH on the viability of the HepG2 cell line. *Journal of Etlik Veterinary Microbiology* **2020**. <https://doi.org/10.35864/evmd.742482>. 983
93. Ichas, F.; Mazat, J.P. From calcium signaling to cell death: two conformations for the mitochondrial permeability transition pore. Switching from low- to high-conductance state. *Biochimica et Biophysica Acta (BBA) - Bioenergetics* **1998**, *1366*, 33–50. [https://doi.org/10.1016/s0005-2728\(98\)00119-4](https://doi.org/10.1016/s0005-2728(98)00119-4). 984
94. Mazzio, E.A.; Boukli, N.; Rivera, N.; Soliman, K.F.A. Pericellular pH homeostasis is a primary function of the Warburg effect: Inversion of metabolic systems to control lactate steady state in tumor cells. *Cancer Science* **2012**, *103*, 422–432. <https://doi.org/10.1111/j.1349-7006.2012.02206.x>. 985
95. Wang, R.; Wang, J.; Hassan, A.; Lee, C.H.; Xie, X.S.; Li, X. Molecular basis of V-ATPase inhibition by bafilomycin A1. *Nature Communications* **2021**, *12*. <https://doi.org/10.1038/s41467-021-22111-5>. 986
96. Masereel, B. An overview of inhibitors of Na/H exchanger. *European Journal of Medicinal Chemistry* **2003**, *38*, 547–554. [https://doi.org/10.1016/s0223-5234\(03\)00100-4](https://doi.org/10.1016/s0223-5234(03)00100-4). 987
97. Tidwell, T.R.; Røslund, G.V.; Tronstad, K.J.; Søreide, K.; Hagland, H.R. Metabolic flux analysis of 3D spheroids reveals significant differences in glucose metabolism from matched 2D cultures of colorectal cancer and pancreatic ductal adenocarcinoma cell lines. *Cancer & Metabolism* **2022**, *10*. <https://doi.org/10.1186/s40170-022-00285-w>. 988
98. Denny, B.J.; Wheelhouse, R.T.; Stevens, M.F.G.; Tsang, L.L.H.; Slack, J.A. NMR and Molecular Modeling Investigation of the Mechanism of Activation of the Antitumor Drug Temozolomide and Its Interaction with DNA. *Biochemistry* **1994**, *33*, 9045–9051. <https://doi.org/10.1021/bi00197a003>. 989